Available online at www.sciencedirect.com
SCIENCE DIRECT®
Journal of Catalysis 226 (2004) 138–155
JOURNAL OF CATALYSIS
www.elsevier.com/locate/jcat

Mechanism of low-temperature selective catalytic reduction of NO with NH_3 over carbon-supported Mn_3O_4 Role of surface NH_3 species: SCR mechanism

Gregorio Marbán *, Teresa Valdés-Solís, Antonio B. Fuertes

Instituto Nacional del Carbón (CSIC), c/Francisco Pintado Fe, 26, 33011 Oviedo, Spain

Received 13 January 2004; revised 17 May 2004; accepted 19 May 2004

Abstract

In this work a complete mechanism for describing the low-temperature (125 °C) selective catalytic reduction of NO with NH_3 over carbon-supported Mn_3O_4 is discussed. This study sets out to explain for the first time certain specific interactions among NH_3, NO, O_2, and a manganese-based catalyst. A set of SCR reactions was obtained through a detailed TPD analysis of the surface NH_3 species and by taking into account the conclusions of a previous study on the role of NO species [Phys. Chem. Chem. Phys. 6 (2004) 453]. The SCR reactions proceed via an Eley–Rideal mechanism, in which NO_2, and to a lesser extent NO, reacts from the gas phase with surface-active NH_3 species. The overall reaction path involves the simultaneous occurrence of two different SCR mechanisms in which either aminooxy groups or ammonium ions react with NO/NO_2. These NH_3-based species are related to the local phases that coexist in Mn_3O_4: (a) SCR by aminooxy groups (steady-state mechanism). Aminooxy groups formed on the locally octahedral environment of Mn_3O_4 (Mn_2O_3) react with gaseous NO_2. O_2 cannot dissociate on this phase in order to reoxidize the reduced catalyst and therefore the overall SCR process is $6NO + 4NH_3 \rightarrow 5N_2 + 6H_2O$. (b) SCR by ammonium ions (pseudo-steady-state mechanism). This mechanism occurs on the locally tetrahedral environment of Mn_3O_4 (MnO) and initially accounts for ∼ 60% of the total NO reduction. However, it is gradually deactivated by the nitrates formed on those same hydroxyl groups that are available for ammonium formation. The ammonium ions formed on the hydroxyl groups of this tetrahedral environment react with gas-phase NO_2. The overall SCR process is $4NO + 4NH_3 + O_2 \rightarrow 4N_2 + 6H_2O$.

Keywords: Selective catalytic reduction; Mechanism; Manganese oxide; Nitric oxide; Ammonia; Vacancies; Aminooxy; Ammonium

1. Introduction

Manganese-based catalysts have attracted widespread interest because their unique redox properties make them useful for a variety of applications. Thus, in recent years, manganese oxides have been proposed as catalysts for several applications such as the oxy-dehydrogenation of propane [1], the selective reduction of nitrobenzene to nitrosobenzene [2], CO oxidation [3], and the low-temperature selective catalytic reduction (SCR) of NO with NH_3 [4–7]. In low-temperature SCR, manganese oxide-based catalysts have been proven to be among the most active catalysts [4,8]. Although low-temperature SCR manganese-based catalysts have been analyzed by several authors [5,9,10] the exact nature of the reaction mechanism remains unclear due in part to the strong NO adsorption that produces partial catalyst deactivation [11]. As a result it is difficult to discern between the species related to the SCR reaction and catalyst deactivation.

In a previous work we carefully analyzed the NO-related species existing on the catalyst surface under low-temperature SCR conditions [11]. In the present study the role of surface NH_3 species is analyzed with the aim of determining the mechanism of the low-temperature selective catalytic reduction of NO with NH_3 over carbon-supported manganese oxide catalysts. This work also provides information which might be of help in understanding the behavior of manganese oxides in other catalytic processes of similar complexity.

* Corresponding author.
E-mail address: greca@incar.csic.es (G. Marbán).

0021-9517/$ – see front matter
doi:10.1016/j.jcat.2004.05.022

2. Summary of previous findings

This section summarizes the previous results relating to the catalytic phase and the formation of NO-related species on the catalyst surface reported in [11] and which are necessary for an understanding of the discussion on the SCR mechanism proposed here. The catalyst chosen for this study is Mn_3O_4 [11] supported on carbon–ceramic cellular monoliths [4] or activated carbon fibers [6,7]. More specifically, the active phase of the catalyst is a nonstoichiometric Mn_3O_4, locally composed of an octahedral Mn_2O_3 phase and a tetrahedral MnO phase, which can be represented by the following empirical formulae (superscripts T and O mean tetrahedral and octahedral, respectively) [11]:

$$Mn_3O_{4+0.5x-y} \Rightarrow \{Mn{=}O\}^{T}_{1-x}\{O{=}Mn{-}O{-}Mn{=}O\}^{T}_{x/2} \{O{=}Mn{-}O{-}Mn{=}O\}^{O}_{1-y}\{O{=}Mn{-}\square{-}Mn{=}O\}^{O}_{y}.$$

This formula accounts for, in order of appearance, the tetrahedral Mn^{2+}–O bonds, the tetrahedral Mn^{3+}–O bonds (oxygen excess), the octahedral Mn^{3+}–O, and the octahedral Mn^{2+}–O bonds (oxygen vacancies), respectively. Fractions x and y have values between 0 and 1, and account respectively for oxygen excess and vacancies in the catalyst.

The nonstoichiometry of the tetroxide is a result of the low temperature used to prepare the catalyst, which gives rise to the oxygen excess bonded to the tetrahedral Mn^{2+}. The distorted structure associated with this oxygen excess may be relaxed by the formation of hydroxyls from water adsorption:

$$2\{Mn{=}O\}^{T} + \tfrac{1}{2}O_2 \leftrightarrow \{O{=}Mn{-}O{-}Mn{=}O\}^{T}, \quad (1)$$

$$\{O{=}Mn{-}O{-}Mn{=}O\}^{T} + 2H_2O \leftrightarrow \{(HO)_2Mn{-}O{-}Mn(OH)_2\}^{T}. \quad (2)$$

The oxygen in the octahedral long Mn^{3+}–O bonds is easily removed by mild-temperature treatments ($\sim 200\,^{\circ}C$) under inert atmosphere. At 125 °C gas-phase oxygen cannot dissociate on the oxygen vacancies of the octahedral environment, but can partly oxidize the tetrahedral MnO phase [11].

The carbonaceous support hardly adsorbs NO at 125 °C. NO adsorbed on Mn_3O_4 is associated with different catalyst centers. NO is weakly adsorbed on octahedral oxygen vacancies as nitrosyls that can dissociate into N_2 when adsorbed in adjacent positions:

$$\{O{=}Mn{-}\square{-}Mn{=}O\}^{O} + NO \leftrightarrow \{O{=}Mn{-}[NO]{-}Mn{=}O\}^{O}, \quad (3)$$

$$2\{O{=}Mn{-}[NO]{-}Mn{=}O\}^{O} \rightarrow 2\{O{=}Mn{-}O{-}Mn{=}O\}^{O} + N_2. \quad (4)$$

This is the main mechanism of catalyst reoxidation at 125 °C. Gas-phase oxygen may indirectly lead to an increase in the amount of surface nitrosyls by generating CO from the carbonaceous support. This reduces the oxidation state of the catalyst, thus increasing the number of oxygen vacancies:

$$\{O{=}Mn{-}O{-}Mn{=}O\}^{O} + CO \rightarrow \{O{=}Mn{-}\square{-}Mn{=}O\}^{O} + CO_2. \quad (5)$$

NO is also adsorbed to a very limited extent as linear (monodentate) and bridged nitrites on the oxygen atoms of the octahedral Mn_2O_3:

$$\{O{=}Mn{-}\square{-}Mn{=}O\}^{O} + NO \leftrightarrow \left\{ \begin{array}{ccc} O & N\cdots O & \\ \| & | & \| \\ Mn\cdots & O & \cdots Mn \end{array} \right\}^{O}. \quad (6)$$

Nitrosyls may react with gas-phase oxygen to produce gas-phase NO_2:

$$\{O{=}Mn{-}[NO]{-}Mn{=}O\}^{O} + \tfrac{1}{2}O_2 \leftrightarrow \{O{=}Mn{-}\square{-}Mn{=}O\}^{O} + NO_2. \quad (7)$$

This reacts with the hydroxyl groups (oxygen excess) of the tetrahedral MnO phase to produce nitrates which, under SCR conditions, cause the progressive deactivation of this catalyst phase:

$$\{(HO)_2Mn{-}O{-}Mn(OH)_2\}^{T} + 6NO_2 \rightarrow \{(NO_3)_2Mn{-}O{-}Mn(NO_3)_2\}^{T} + 2H_2O + 2NO. \quad (8)$$

3. Experimental

3.1. Catalysts

The preparation of the catalysts is described in detail elsewhere [4,6,7,11]. The following catalysts were prepared by equilibrium adsorption impregnation: (i) a carbon–ceramic monolith-supported manganese oxide catalyst (CCCM-Mn; Mn content on a carbon basis = 7.1 ± 0.9 wt%), whose activated support will be denoted as CCCM-40 (the numerical suffix in the reference indicates the carbon weight loss after steam activation), and (ii) an activated carbon fiber composite-supported manganese oxide catalyst (ACFC-Mn; Mn content in carbon basis = 4.8 wt%) prepared by impregnation of the steam-activated support (ACFC-20). For all experiments performed with CCCM-40 or ACFC-20 (FTIR, TPD, etc.) the samples were previously oxidized with nitric acid and heat treated in N_2 at 400 °C for 1 h [11]. The effective size of the supported carbon layer in CCCM was found to vary in the range 10–20 μm.

3.2. Step-response and temperature-programmed desorption (TPD) experiments

Samples of CCCM-40 supports and CCCM-Mn catalysts, crushed to a particle size below 1 mm, were tested for adsorption/desorption/reactions under different gas atmospheres and temperature programs in a vertical quartz reactor (0.65 cm i.d.) connected to an Omnistar model mass

Table 1
Deconvolution parameters for the NO and NH_3 evolution curves during the TPD stage averaged for all the experiments

Gas	Starting TPD temperature (°C)	LT peak			MT peak			HT peak		
		T_{LT} (°C)	Ea_{LT} (kJ mol^{-1})	n_{LT}	T_{MT} (°C)	Ea_{MT} (kJ mol^{-1})	n_{MT}	T_{HT} (°C)	Ea_{HT} (kJ mol^{-1})	n_{HT}
NO	125	177 ± 6	Fig. 3 in [11]	1.6	–	–	–	231 ± 8	Fig. 3 in [11]	1.8 ± 0.2
	175	201 ± 11	92 ± 10	1.6	–	–	–	242 ± 6	132 ± 6	1.8 ± 0.5
NH_3	125	204 ± 5	79 ± 5	2.0	262 ± 4	67 ± 1	1.5	370 ± 12	60 ± 1	1.6
	175	255 ± 8	90 ± 4	2.0	322 ± 4	60 ± 1	1.5	403 ± 4	63	1.6

spectrometer. A typical sample mass of 1 g and a gas flow rate of 150 mL (STP) min^{-1} were used during the experiments. By means of a combination of mass-flow controllers it was possible to obtain different mixtures of NO, NH_3, and O_2 in He. A typical experiment comprised four stages: (1) *degasification* of the sample in He at 200 °C for 30 min, (2) single or multiple *step-response* experiments (see below), (3) *isothermal desorption* in He at the temperature of the final step-response experiment, and (4) *temperature-programmed desorption* in He (TPD stage) at 5 °C min^{-1} up to 400 °C. Step-response experiments were performed at 125 and 175 °C, and the response of the system to a given combination of different gases (700 ppm NO; 800 ppm NH_3; 3 vol% O_2; 3.3 vol% H_2O and He) was analyzed. With this experimental procedure the entire experiment could be labeled with reference only to the step-response stage, since the other stages were always performed in the same manner. Thus, an experiment referred to as $NO + O_2{}^{125\,^\circ C}{}_{60} > NH_3{}^{125\,^\circ C}{}_{40}$ consisted of stages 1, 3, and 4 as described above, and a step-response sequence (stage 2) comprising a first step under NO + O_2 atmosphere (700 ppm NO, 3 vol% O_2 in He) at 125 °C for 60 min followed by a second step under NH_3 atmosphere (800 ppm NH_3 in He) at 125 °C for 40 min.

4. Results and discussion

4.1. Procedure for the quantification of the adsorbed species

Both the NO and the NH_3 evolution curves during the TPD step were subjected to a numerical fitting procedure with the purpose of finding convolved Arrhenius-type curves [12]. The procedure consisted in finding a minimum number of Arrhenius-type curves whose convolution would closely resemble the experimental curve, and at the same time show features common to all the performed experiments. For the NO curves these premises can be fulfilled by taking only two desorption peaks, a low-temperature peak (LT peak) and a high-temperature peak (HT peak) [11]. For the NH_3 evolution curves during the TPD experiments three characteristic peaks are needed for a satisfactory agreement: an LT (low-temperature) peak, an MT (medium-temperature) peak, and an HT (high-temperature) peak (examples of these are not included for brevity). The values of maximum peak temperature (T_i), activation energy (E_{a_i}), and reaction order (n_i) for these peaks averaged for all the experiments performed are shown in Table 1. The values of the peak areas obtained for the different experiments are displayed in Table 2 for the NO curves and in Table 3 for the NH_3 curves. In these tables the parameter Φ_{NO}^{TPD} ($\Phi_{NH_3}^{TPD}$) means the total moles of desorbed NO (NH_3) per manganese moles in the sample during the *TPD stage*, whereas Φ^{LT}, Φ^{MT}, and Φ^{HT} represent the moles of desorbed NO or NH_3 per manganese moles ascribed to low-temperature (LT), medium-temperature (MT), and high-temperature peak (HT), respectively. Additionally, these tables include the values of NO/NH_3 desorbed during the *isothermal desorption stage* per manganese moles (Φ^{iso}) for all the experiments, and the values of N_2 formed during the TPD stage per manganese moles ($\Phi_{N_2}^{TPD}$) for selected experiments, values that have already been discussed in the case of NO [11].

The data displayed in Tables 2 and 3 are the main basis for the subsequent discussions on NO- and NH_3-based species that coexist on the catalyst surface under different conditions.

4.2. NH_3 adsorption/reaction modes: SCR mechanism

4.2.1. Adsorption of NH_3 by the carbonaceous support

It can be seen from Table 3 that the carbonaceous support itself adsorbs a significant amount of NH_3 (codes h0, i0, d0, 11, 12), although the quantity is lower than that adsorbed by the catalyst. Generally speaking, a clean carbon surface is considered to have a basic character, so that ammonia must be adsorbed on acidic functional groups formed on the support surface [13,14]. It is well known that nitric oxidation of a carbon surface at moderate temperatures increases surface acidity mainly through the creation of carboxylic functional groups, although other less acidic groups such as phenols and lactones are also formed. From the values provided by the literature [15] and taking into account the fact that the heat treatment performed after the oxidation step of CCCM-40 is strong enough to decompose single carboxylic groups to CO_2 and to dehydrate adjacent carboxylic and phenolic groups to anhydrides or lactones [16], it is possible to

Table 2
Moles of NO (isothermal desorption stage (Φ_{NO}^{iso}) and TPD (Φ_{NO}^{TPD})) and N_2 (TPD ($\Phi_{N_2}^{TPD}$)) released per manganese moles in the catalysts during the experiments

Code	Sample	Step-response sequence	Φ_{NO}^{iso}	Φ_{NO}^{TPD}		$\Phi_{N_2}^{TPD}$
				Φ_{NO}^{LT}	Φ_{NO}^{HT}	
1[a]	CCCM-40	$NO^{125\,°C}{}_{66}$	0.007		0.004	–
2[a]	CCCM-40	$NO + O_2{}^{125\,°C}{}_{60}$	0.008		0.004	–
3[a]	CCCM-40	$NO + O_2 + NH_3{}^{125\,°C}{}_{59}$	0.020		0.010	–
a2	CCCM-Mn	$NO^{125\,°C}{}_{93}$	0.023	0.010	0.001	0.004
b1	CCCM-Mn	$NO + O_2{}^{125\,°C}{}_{15}$	0.064	0.002	0.091	–
b2	CCCM-Mn	$NO + O_2{}^{125\,°C}{}_{137}$	0.017	0.017	0.191	0.010
f	CCCM-Mn	$NO + O_2 + H_2O^{125\,°C}{}_{115}$	0.021	0.000	0.047	–
8	CCCM-Mn	$NO^{175\,°C}{}_{64}$	0.017	0.002	0.000	–
9	CCCM-Mn	$NO + O_2{}^{175\,°C}{}_{131}$	0.032	0.002	0.075	–
10	CCCM-Mn	$NO + O_2 + H_2O^{175\,°C}{}_{81}$	0.026	0.000	0.004	–
d1	CCCM-Mn	$NO + O_2 + NH_3{}^{125\,°C}{}_{10}$	0.101	0.009	0.006	0.009
d2	CCCM-Mn	$NO + O_2 + NH_3{}^{125\,°C}{}_{20}$	0.102	0.014	0.016	0.019
d3	CCCM-Mn	$NO + O_2 + NH_3{}^{125\,°C}{}_{45}$	0.064	0.014	0.022	0.019
d4	CCCM-Mn	$NO + O_2 + NH_3{}^{125\,°C}{}_{60}$	0.035	0.004	0.032	0.027
d5	CCCM-Mn	$NO + O_2 + NH_3{}^{125\,°C}{}_{120}$	0.030	0.004	0.060	0.026
e2	CCCM-Mn	$O_2{}^{125\,°C}{}_{64} > NO^{125\,°C}{}_{57}$	0.046	0.009	0.000	–
e3	CCCM-Mn	$O_2{}^{175\,°C}{}_{45} > NO^{125\,°C}{}_{68}$	0.048	0.015	0.000	–
j[b]	CCCM-Mn	$NO + O_2{}^{125\,°C}{}_{90} > NH_3{}^{125\,°C}{}_{91}$	0.018	0.000	0.197	0.080
c	CCCM-Mn	$NH_3{}^{125\,°C}{}_{97} > NO^{125\,°C}{}_{94}$	0.030	0.014	0.002	0.006
k	CCCM-Mn	$NH_3{}^{125\,°C}{}_{90} > NO + O_2{}^{125\,°C}{}_{100}$	0.054	0.020	0.204	0.019
g	CCCM-Mn	$NH_3 + O_2{}^{125\,°C}{}_{94} > NO^{125\,°C}{}_{101}$	0.030	0.008	0.006	0.007
a1, e[c]	CCCM-Mn	$NO^{125\,°C}{}_{30} > He^{125\,°C}{}_{15} > O_2{}^{125\,°C}{}_{85} > He^{125\,°C}{}_{15} > NO^{125\,°C}{}_{30} > He^{125\,°C}{}_{15} > O_2{}^{125\,°C}{}_{30}$	0.046	0.020	0.004	–

See Table 1 for peak temperatures.
[a] Values of Φ evaluated by assuming a hypothetical Mn load equal to that of the corresponding experiments with CCCM-Mn.
[b] Isothermal desorption after the NH_3 adsorption stage ($\Phi_{NO}^{iso} = 0.039$ after the $NO + O_2$ adsorption stage).
[c] Isothermal desorption after the last NO adsorption stage ($\Phi_{NO}^{iso} = 0.014$ after the first NO adsorption stage).

estimate the approximate molar distribution of oxygen functional groups: ∼ 2–6 mmol g^{-1} = ∼ 65% carbonyls (basic groups), ∼ 15% phenolics, ∼ 20% (anhydrides + lactones). The total amount of NH_3 desorbed by CCCM-40 after $NH_3{}^{125\,°C}{}_{64}$ (code h0 of Table 3) is ∼ 0.2 $mmol_{NH_3}\ g_C^{-1}$, which means that, if the basic carbonyls are not adsorbing NH_3, a moderate proportion of available oxygen surface groups are performing the adsorption (∼ 10–30%). Anhydrides and lactones can physisorb NH_3 via weak hydrogen bonding on the oxygen atoms of –O–C=O groups, which may partially evolve to yield more strongly bonded amine-type species [17]. On the other hand, phenolic groups adsorb NH_3 via acid–base interaction to produce ammonium ions linked to oxygen atoms [17]. In the isothermal desorption stage used in our experiments, after the NH_3 step, the samples were left under a He atmosphere for ∼ 30 min at 125 °C (175 °C in certain cases) so that, in accordance with the literature [18,19], most of the NH_3 weakly adsorbed on oxygen atoms via hydrogen bonding can be expected to be released in this stage, both for the catalysts and for the supports. Robb et al. [19] also established by means of combined NH_3-STPD and FTIR that the thermal stability ranges of NH_3 bonded as NH_4^+ to Brønsted hydroxyl groups on Si and Al atoms of zeolites can be defined by desorption peaks located at 350, 440, and 540 °C. By combining the work of Chughtai et al. [17] with the works on zeolites [18,19], we can tentatively assign the different NH_3 adsorption modes on the CCCM-40 support as follows: (i) NH_3 adsorbed via hydrogen bonding to anhydrides and lactones is released in the isothermal desorption stage; (ii) the LT peak is originated by the liberation of reactively adsorbed ammonia (possibly NH_2 species produced by hydrogen abstraction of weakly adsorbed NH_3), and (iii) the MT and HT peaks (peak temperatures for experiments at 175 °C: 322, and 403 °C, respectively) are formed by the desorption of NH_3 linked as ammonium ions to phenolic groups of varying acid strength.

Table 3
Moles of NH_3 (isothermal desorption stage ($\Phi^{iso}_{NH_3}$) and TPD ($\Phi^{TPD}_{NH_3}$)) and N_2 (TPD ($\Phi^{TPD}_{N_2}$)) released per manganese moles in the catalysts during the experiments

Code	Sample	Step-response sequence	$\Phi^{iso}_{NH_3}$	$\Phi^{TPD}_{NH_3}$			$\Phi^{TPD}_{N_2}$
				$\Phi^{LT}_{HN_3}$	$\Phi^{MT}_{NH_3}$	$\Phi^{HT}_{NH_3}$	
h0[a]	CCCM-40	$NH_3{}^{125\,^\circ C}{}_{64}$	0.079	0.031	0.014	0.015	–
i0[a]	CCCM-40	$NH_3 + O_2{}^{125\,^\circ C}{}_{60}$	0.055	0.028	0.016	0.015	–
d0[a]	CCCM-40	$NO + O_2 + NH_3{}^{125\,^\circ C}{}_{59}$	0.064	0.035	0.016	0.016	–
11[a]	CCCM-40	$NH_3{}^{175\,^\circ C}{}_{60}$	0.032	0.018	0.012	0.008	–
12[a]	CCCM-40	$NH_3 + O_2{}^{175\,^\circ C}{}_{131}$	0.078	0.035	0.023	0.016	–
h1	CCCM-Mn	$NH_3{}^{125\,^\circ C}{}_{112}$	0.156	0.102	0.042	0.023	–
i1	CCCM-Mn	$NH_3 + O_2{}^{125\,^\circ C}{}_{119}$	0.136	0.088	0.045	0.032	–
m	CCCM-Mn	$NH_3 + O_2 + H_2O^{125\,^\circ C}{}_{122}$	0.011	0.047	0.029	0.018	–
13	CCCM-Mn	$NH_3{}^{175\,^\circ C}{}_{83}$	0.171	0.077	0.009	0.021	–
14	CCCM-Mn	$NH_3 + O_2{}^{175\,^\circ C}{}_{125}$	0.071	0.076	0.035	0.053	–
15	CCCM-Mn	$NH_3 + O_2 + H_2O^{175\,^\circ C}{}_{122}$	0.003	0.034	0.025	0.058	–
d1	CCCM-Mn	$NO + O_2 + NH_3{}^{125\,^\circ C}{}_{10}$	0.082	0.051	0.018	0.012	0.009
d2	CCCM-Mn	$NO + O_2 + NH_3{}^{125\,^\circ C}{}_{20}$	0.092	0.069	0.024	0.017	0.019
d3	CCCM-Mn	$NO + O_2 + NH_3{}^{125\,^\circ C}{}_{45}$	0.092	0.094	0.037	0.018	0.019
d4	CCCM-Mn	$NO + O_2 + NH_3{}^{125\,^\circ C}{}_{60}$	0.117	0.097	0.023	0.019	0.027
d5	CCCM-Mn	$NO + O_2 + NH_3{}^{125\,^\circ C}{}_{120}$	0.131	0.110	0.017	0.017	0.026
16	CCCM-Mn	$NO + O_2 + NH_3{}^{175\,^\circ C}{}_{75} > NO + NH_3{}^{175\,^\circ C}{}_{134}$	0.113	0.040	0.022	0.029	–
j	CCCM-Mn	$NO + O_2{}^{125\,^\circ C}{}_{90} > NH_3{}^{125\,^\circ C}{}_{91}$	0.178	0.118	0.003	0.013	0.080
c	CCCM-Mn	$NH_3{}^{125\,^\circ C}{}_{97} > NO^{125\,^\circ C}{}_{94}$	0.187 + 0.006[b]	0.000	0.032	0.017	0.006
k	CCCM-Mn	$NH_3{}^{125\,^\circ C}{}_{90} > NO + O_2{}^{125\,^\circ C}{}_{100}$	0.158 + 0.004[b]		0.002		0.019
g	CCCM-Mn	$NH_3 + O_2{}^{125\,^\circ C}{}_{94} > NO^{125\,^\circ C}{}_{101}$	0.115 + 0.005[b]	0.000	0.014	0.013	0.007

See Table 1 for peak temperatures.
[a] Values of Φ evaluated by assuming a hypothetical Mn load equal to that of the corresponding experiments with CCCM-Mn.
[b] NH_3 desorption during the NO/NO + O_2 step + NH_3 desorption during the isothermal desorption stage.

4.2.2. *NH_3 weakly adsorbed by the catalyst ($\Phi^{iso}_{NH_3}$)*

Fig. 1 shows the NH_3-TPD curves for the experiments of NH_3 adsorption at 125 and 175 °C performed on both the catalyst and the carbonaceous support where similar profiles for both materials are observed with almost identical maximum reactivity temperatures. The TPD curve corrected for the support ((h1)–(h0) in Fig. 1) yields a similar profile. Furthermore, the NH_3-TPD curves obtained for the support could be resolved by using the same peak distribution and kinetic parameters as those determined for the catalyst (Table 1). This suggests strongly that for both the support and the catalyst similar functionalities are used to link the NH_3-based species, oxygen atoms being the only functionalities common to both materials. However, several authors [5,9,10] consider that NH_3 is adsorbed predominantly on oxygen vacancies of transition metal oxides, such as those used for linking NO in the form of nitrosyls. In this case competition between both gases might be expected to occur. However, from the results shown in Table 2 the opposite effect can be observed; the experiments in which ammonia was passed prior to or together with NO gave rise to the enhanced desorption of NO from nitrosyls in the isothermal stage. In conclusion, at 125 °C the oxygen vacancies of Mn_3O_4 ad-

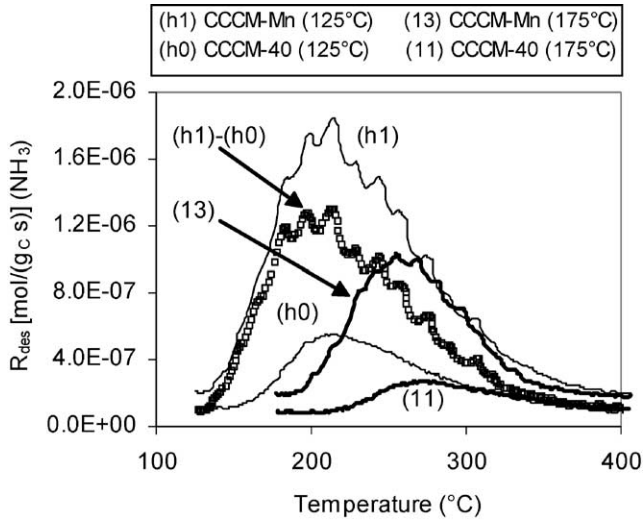

Fig. 1. Rates of NH_3 release on a carbon mass basis during the TPD stage of the experiments of NH_3 adsorption at 125 °C ($NH_3{}^{125\,^\circ C}{}_{60–110}$) and 175 °C ($NH_3{}^{175\,^\circ C}{}_{60–80}$) with CCCM-40 and CCCM-Mn. Open squares: CCCM-Mn curve corrected for CCCM-40 ($NH_3{}^{125\,^\circ C}$) (codes as in Table 3).

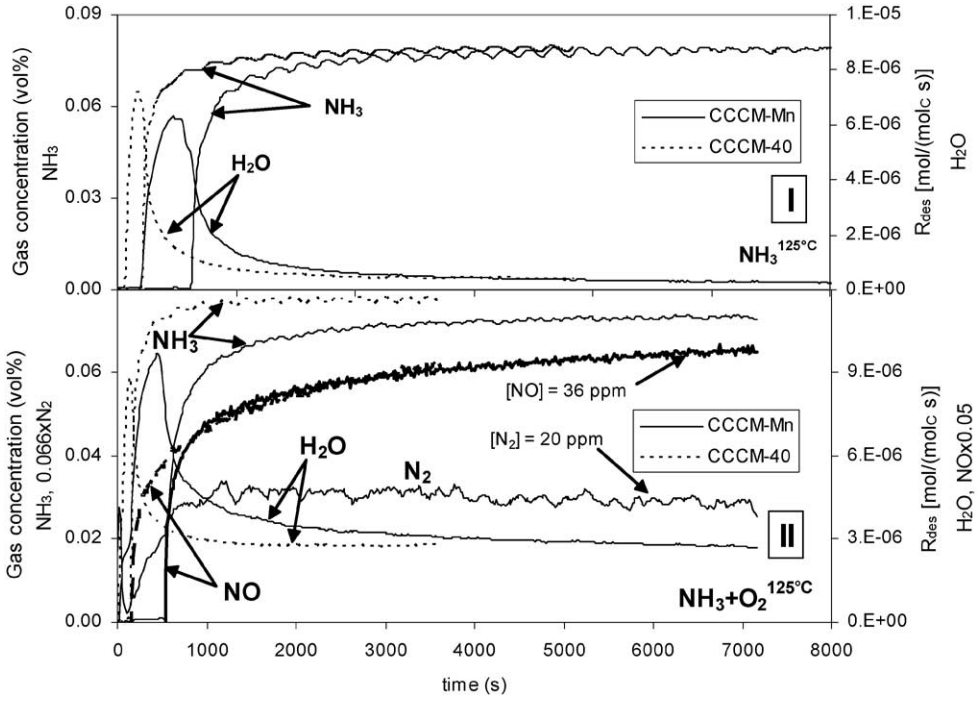

Fig. 2. Evolution with time of NH_3 and H_2O gas concentration and NO desorption rate based on carbon content during the step-response stage of $NH_3{}^{125\,^\circ C}$ (I) and $NH_3 + O_2{}^{125\,^\circ C}$ (II) experiments for CCCM-40 and CCCM-Mn.

sorb acid NO molecules but do not seem to adsorb basic NH_3 molecules. This can be expected for electron-donor defects, examples of which are the oxygen vacancies of ZrO_{2-y} or Nb_2O_{5-y} [16], which preferentially adsorb acid-type molecules. A final piece of evidence that shows the preferred adsorption of ammonia on oxygen atoms is indirectly provided by comparing NO–H_2O competition with NH_3–H_2O competition on CCCM-Mn. As regards the former, water completely impedes the formation of species ascribed to the LT peak of the NO-TPD (code f in Table 2), due to the competitive adsorption on the oxygen atoms [11]. Since H_2O also impedes the weak adsorption of NH_3 (codes m and 15 in Table 3) it follows that this process must take place on the oxygen atoms.

The results above lead to the conclusion that ammonia is preferentially linked to the oxygen atoms of manganese oxides. Certain works also propose oxygen–ammonia intermediates for the SCR reaction [21–25]. It can be assumed therefore that NH_3 which desorbs at 125 °C during the isothermal desorption stage corresponds to weakly adsorbed NH_3 on the oxygen atoms of manganese oxide via hydrogen bonding. In principle this bonding is performed on the octahedral phase of the oxide, $\{O{=}Mn{-}O{-}Mn{=}O\}^O$, since MnO seems to be a poor NH_3 adsorbent. In this respect, an $NH_3 + NO^{175\,^\circ C}$ experiment over pure MnO particles (not shown) yielded negligible NH_3 adsorption during the step-response stage. As pointed out previously, coadsorption of H_2O produces a strong decrease in the amount of weakly adsorbed NH_3 (code m in Table 3), indicating that water is able to establish stable hydrogen bonds with the oxygen atoms of the manganese oxides. When NH_3 is passed through the catalyst, a significant amount of water is also released by the catalyst (Fig. 2). For long reaction times (3000–4000 s), when NH_3 is no longer being adsorbed, the water is only released from the carbonaceous support. Once the amount of water desorbed by the carbonaceous support has been subtracted from that desorbed by the catalyst, the resulting amount is the same in both the absence or the presence of oxygen. Consequently the similarity of the curve shapes and the amounts of desorbed water for the $NH_3{}^{125\,^\circ C}$ and $NH_3 + O_2{}^{125\,^\circ C}$ experiments suggests that the source of water is the same in both cases. For the $NH_3{}^{125\,^\circ C}$ experiment only two possible sources are available: (i) the reaction of surface oxygen with the hydrogen atoms of either the adsorbed ammonia or surface hydroxyls, and (ii) the competition of ammonia with weakly bonded water on the oxygen atoms of the manganese oxide. If it were the first route, the elimination of surface oxygen in the form of water molecules would be accompanied by the creation of oxygen vacancies on the catalyst surface.

In a previous work [11] we established an indirect way of assessing the amount of oxygen vacancies on the surface of the catalyst by determining the amount of N_2 formed in the initial moments of the NO(+O_2) step. Fig. 3 offers the N_2 release rates during the NO(+O_2) steps (in square brackets in the legend) of different experiments. As can be observed, a NH_3 step before the introduction of NO produces a significant increase in the formation of N_2, from $\Phi_{N_2} = 0.002$ to 0.108. Most of this nitrogen comes from the SCR reaction of NO with preadsorbed ammonia, specifically with all the ammonia species ascribed to the LT peak of the TPD curve and some of the ammonia species ascribed to the MT and

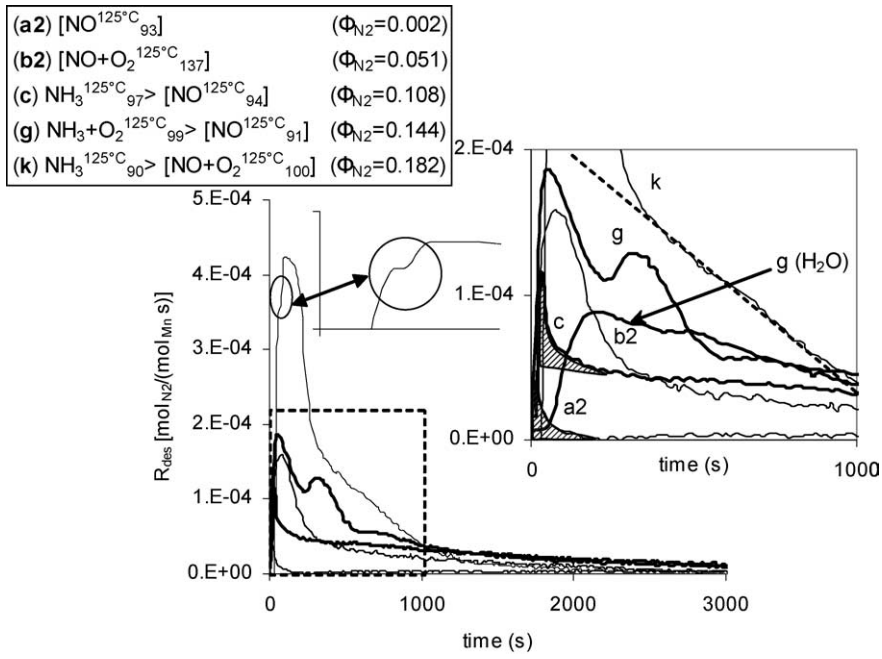

Fig. 3. Evolution of N_2 concentration in the exit gases during the NO(+O_2) step (in brackets) of experiments performed with CCCM-Mn. The inset is an enlarged image of the dashed box section (codes as in Table 2).

HT peaks. Thus the amount of N_2 formed during the passage of NO (Fig. 3; $\Phi_{N_2} = 0.108$) is very similar to the amount of NH_3 desorbed at the LT peak of the $NH_3{}^{125\,^\circ C}$ experiment (code h1 of Table 3; $\Phi^{LT}_{NH_3} = 0.102$), a peak which is absent in the TPD curve of the $NH_3{}^{125\,^\circ C} > NO^{125\,^\circ C}$ experiment. In this experiment, therefore, the oxygen vacancies are only responsible for a minute contribution to the total N_2 released during the passage of NO. By comparing curves c and a2 in Fig. 3 (inset) it can be concluded that only the shaded areas are related to the nitrogen formed by a direct NO reaction on the oxygen vacancies. The similarity of both areas implies that no oxygen vacancies were created during the NH_3 step. If oxygen is introduced together with NH_3 before the NO step, then a sharper N_2 peak appears in the initial moments of the NO step (curve g in Fig. 3). The N_2 peak is not accompanied by a parallel water release (curve g (H_2O) in Fig. 3), which means that it is produced by a reduction of NO on the oxygen vacancies rather than an SCR reaction with preadsorbed NH_3. Nevertheless, this peak is almost coincident with that produced during the NO + O_2 experiment (curve b2 in Fig. 3). The oxygen vacancies are therefore created by CO produced by oxygen oxidation of the carbonaceous surface [11] during the $NH_3 + O_2$ step and not by the action of NH_3.

In conclusion, the adsorption of NH_3 does not produce oxygen vacancies on the manganese oxide, and so the concomitant water release during the passage of NH_3 (Fig. 2I) must correspond to H_2O weakly adsorbed on the oxygen atoms of the manganese oxide that has survived the catalyst pretreatment. The following equilibrium equation is introduced to illustrate these results:

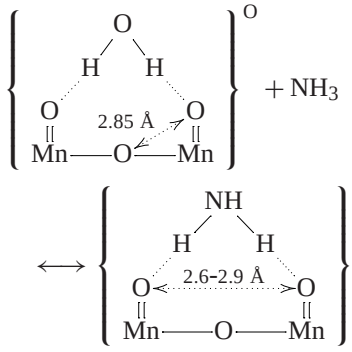

(9)

In the above representation of the octahedral Mn_2O_3 phase, the Mn–O–Mn bonds represent the long and labile Mn–O bonds (1/3 of this phase) which are a precursor of the oxygen vacancies [11], whereas Mn=O represents the short Mn–O bonds (2/3 of this phase). The distances between both kinds of oxygen atoms [26] are indicated in the equation, the H–H distances of H_2O and NH_3 being represented on the same scale as the =O =O distance. NH_3 is assumed to be adsorbed on the short Mn=O bonds since adsorption on the labile oxygen atoms would imply a significant decrease in NH_3 adsorption at 125 °C, when O_2 is present in the gas phase, as a consequence of the formation of oxygen vacancies. This decrease was not observed in any of the experiments (points h1 vs i1 in Fig. 4II).

As can be observed in Fig. 2I, in the absence of O_2 and NO, the release of water from CCCM-Mn starts at ∼ 200 s (ammonia being first adsorbed on the water-free sites) and finishes at ∼ 3000 s. This means that attaining equilibri-

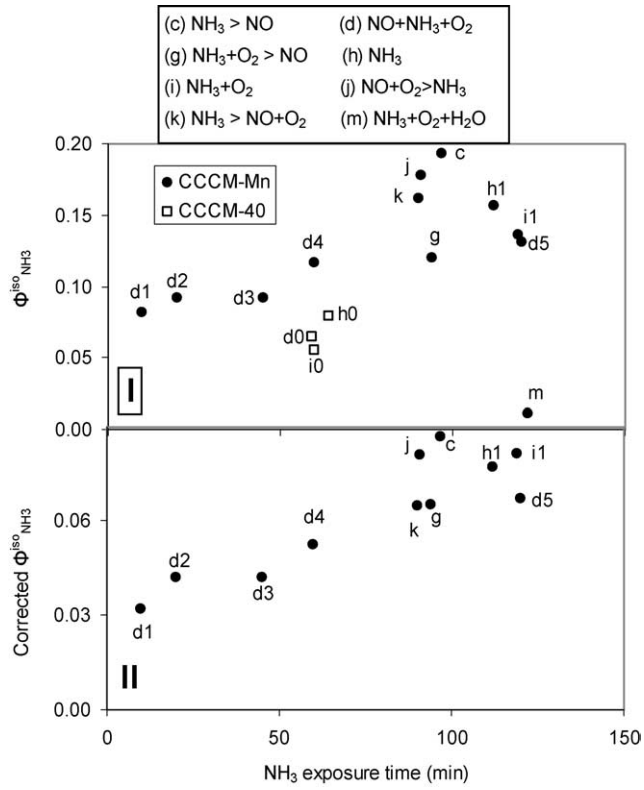

Fig. 4. Moles of desorbed NH_3 per manganese moles versus NH_3 exposure time for: (I) isothermal desorption after the $NH_3(+O_2(+H_2O))$ stage, (II) isothermal desorption corrected for desorption by the support. The legends indicate the corresponding step-response sequences at 125 °C performed over CCCM-Mn (codes as in Table 3).

um (9) is a slow process. After an NH_3 or $NH_3 + O_2$ step the amounts of desorbed NH_3 in He ($\Phi^{iso}_{NH_3}$; codes h1 and i1 in Table 3) are similar to those determined in NO or in $NO + O_2$ ($\Phi^{iso}_{NH_3}$; codes c, k, and g in Table 3). This suggests that weakly adsorbed NH_3 does not directly react with NO or $NO + O_2$, as do the ammonia species ascribed to the different TPD peaks.

Fig. 4I plots the experimental values of $\Phi^{iso}_{NH_3}$ vs the NH_3 exposure time for all the experiments performed with NH_3. The plotted values (indicated in Table 3) correspond to the desorption of NH_3 under the gas atmosphere of the stage that followed the passage of NH_3 (He in d, h, i, j, and m). As the amount of ammonia adsorbed by the support was quite high, it was necessary to subtract its value from the overall amount adsorbed by the catalyst in order to estimate properly the amount of NH_3 desorbed by the active phase. These results are plotted in Fig. 4II, where the increasing trend of $\Phi^{iso}_{NH_3}$ with NH_3 exposure time can easily be appreciated. The points that clearly make up this trend are d1 to d4 ($NO + NH_3 + O_2$ experiments), whose lower $\Phi^{iso}_{NH_3}$ values with respect to the other points may be explained in two ways: (i) by the previously noted slowness of the NH_3 adsorption–water displacement process (9); (ii) by a transient reaction of weakly adsorbed NH_3 toward an active species in the SCR process. Both explanations are probably valid, since the water displacement process is no longer significant at exposure times of over ~ 30 min (Fig. 2II) and the weakly adsorbed NH_3 has not yet reached its attainable maximum under SCR conditions (Fig. 4II). Nevertheless, the fact that for long exposure times the amount of weakly adsorbed NH_3 in the absence of water is approximately constant regardless of the composition of the atmosphere (corrected $\Phi^{iso}_{NH_3} = 0.075 \pm 0.009$) supports the assumption that weakly adsorbed NH_3 on water-free sites or via equilibrium (9) is not the active ammonia species in an SCR reaction.

On the other hand, weakly adsorbed NH_3 does appear to react partly with gas-phase oxygen, as can be deduced from the decrease in $\Phi^{iso}_{NH_3}$ when oxygen is introduced together with NH_3, especially at 175 °C (codes 13 vs 14 in Table 3). Fig. 2II shows that during the passage of $NH_3 + O_2$ at 125 °C, NH_3 is converted into NO at the same conversion degree by both the catalyst and the carbonaceous support. This means that oxidation of NH_3 to NO is only catalyzed by the support. The gas-phase oxidation of NH_3 can be disregarded since NO is not released from $t = 0$ (Fig. 2II). In any case, the carbon-catalyzed oxidation of NH_3 to NO only

Table 4
Total moles of NO, N_2, and N_2O per carbon moles released during the different $NH_3(+O_2(+H_2O))$ stages after 60 min reaction

Sample	T (°C)	Stage	Gas/C = mol gas/mol C		
			NO/C (%NH_3)[a]	N_2/C (%NH_3)[a]	N_2O/C (%NH_3)[a]
CCCM-40	125	NH_3	0	0	0
		$NH_3 + O_2$	1.3×10^{-3} (3.1%)	0	0
	175	NH_3	0	0	0
		$NH_3 + O_2$	1.9×10^{-3} (4.4%)	6.6×10^{-4} (3.5%)	3.3×10^{-4} (0.6%)
CCCM-Mn	125	NH_3	0	0	0
		$NH_3 + O_2$	1.3×10^{-3} (4.2%)	8.2×10^{-4} (4.3%)	2.1×10^{-4} (0.7%)
		$NH_3 + O_2 + H_2O$	3.6×10^{-4} (1.3%)	0	0
	175	NH_3	0	0	0
		$NH_3 + O_2$	9.3×10^{-4} (2.9%)	1.7×10^{-3} (10.1%)	6.9×10^{-4} (5.5%)
		$NH_3 + O_2 + H_2O$	2.9×10^{-4} (1.2%)	0	0

[a] Percentage of inlet NH_3 consumed to give the corresponding gas at $t = 60$ min (pseudo-steady state).

produces a diminution of ∼ 1–4 vol% in the inlet NH_3 concentration under all the conditions studied. This is shown in Table 4, where the amounts of N_2, N_2O, and NO formed in 1 h of the $NH_3(+O_2(+H_2O))$ stages at 125 and 175 °C for both the catalyst and the support are presented. For the sake of comparison, the steady-state conversion of NH_3 to N_2 at 125 °C under SCR conditions was in the range of 50–60%. The low NH_3 reaction to NO cannot possibly explain the high decrease in weakly adsorbed NH_3 at 175 °C when oxygen is present. This can only be explained by the reaction of adsorbed NH_3 with O_2 to give N_2 and, to a lesser extent, N_2O, which is only (125 °C) or mainly (175 °C) catalyzed by the active phase, as can be inferred from the values indicated in Table 4. The SCR reaction of NO that evolves from the carbonaceous surface with the adsorbed NH_3-derived species can be rejected as a potential source of the observed N_2 (at least to any significant extent) since this gas was detected from the very beginning of the stage and NO starts to be released to the gas phase at $t \approx 550$ s (Fig. 2II). In the next section it will be proved that the adsorbed NO does not react with NH_3 to produce N_2 (*LH vs ER mechanism* section). The following reactions of direct oxidation are therefore considered:

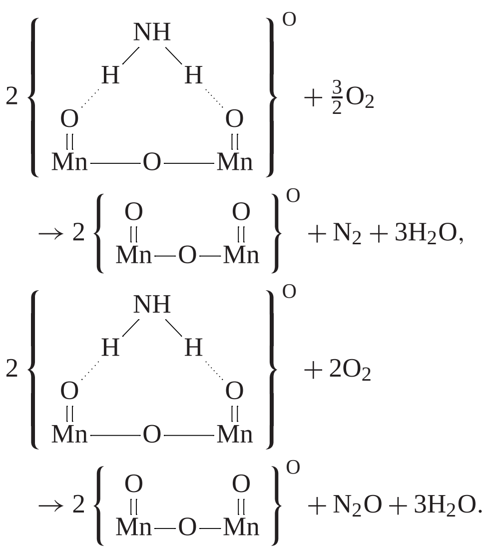

(10)
(11)

According to Table 4, reaction (10) can convert around 10% of the inlet NH_3 into N_2 at 175 °C (SCO reaction [27]), the temperature at which reaction (11) also starts to become noticeable (∼ 5% conversion of NH_3). The fact that the presence of water inhibits both reactions (Table 4) is yet further proof that reactions (10) and (11) are produced from weakly adsorbed NH_3, displaced from the surface by water (codes m and 15 in Table 3), and not from the more stable ammonia-derived species desorbed during the TPD stage. It is not surprising that NO is not produced by NH_3 oxidation on the active phase, since this reaction is known to occur at higher temperatures than those needed for reactions (10) and (11) [27]. Finally, the NO that evolves from the carbonaceous surface after NH_3 oxidation may be partly adsorbed as nitrosyls on the surface of the active phase (3), then converted to NO_2 (7), and eventually stored as nitrates in the tetrahedral phase of the catalyst (8). This mechanism would explain the small though conspicuous HT peak found in the NO-TPD of the $NH_3+O_2{}^{125\,°C}{}_{94} > NO^{125\,°C}{}_{101}$ experiment (code g in Table 2).

4.2.3. LH vs ER mechanism: NO–NH$_3$ competition

As noted in [11], there is still some controversy as to the state of NO when it reacts with NH_3 at low temperatures. There is a broad consensus regarding the fact that NH_3 always reacts from an adsorbed state, but results from various sources suggest that the NO state (gaseous or adsorbed) when reacting with adsorbed NH_3 depends on the catalytic system [5,9,10,28,29]. At this stage of the discussion we are in position to determine for CCCM-Mn whether NO reacts from the gas phase (ER mechanism), from an adsorbed state (LH or Freundlich mechanism), or by a combined ER-LH mechanism. An assessment can be reached by analyzing the results of a specific step-response experiment. Fig. 5I displays the evolution of the N_2 and NO concentrations during the step-response stages of $NO + O_2{}^{125\,°C}{}_{90} > NH_3{}^{125\,°C}{}_{91}$. In the first stage N_2 is produced by NO reduction on the oxygen vacancies of the catalyst. When the passage of $NO + O_2$ is stopped and NH_3 is introduced, the production of N_2 ceases, even though the catalyst surface is covered with nitrosyls, nitrites, and nitrates. This is strong evidence that NO must be in the gas phase to react with adsorbed NH_3. Further support for this hypothesis is provided by the TPD results of

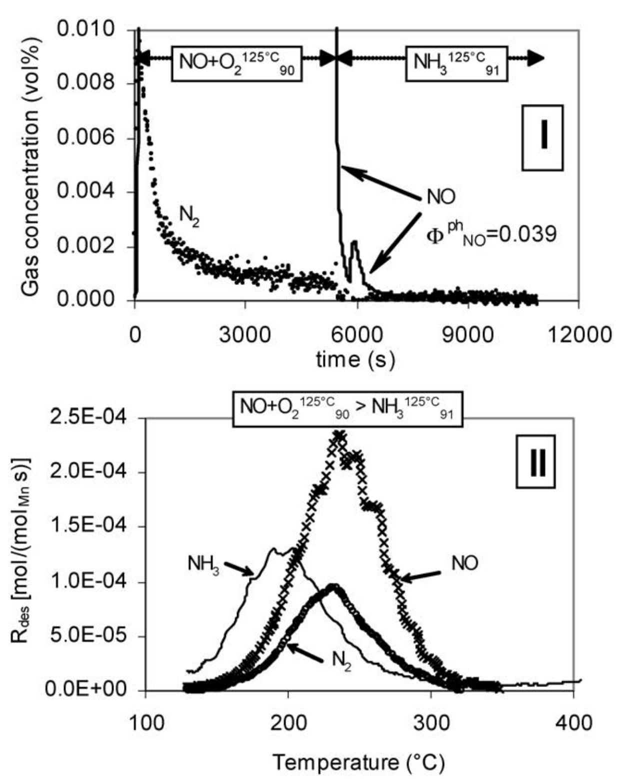

Fig. 5. Results of the $NO + O_2{}^{125\,°C}{}_{90} > NH_3{}^{125\,°C}{}_{91}$ experiment: (I) Evolution of N_2 and NO during the step-response stage. (II) Evolution of NH_3, NO, and N_2 during the TPD stage (codes as in Table 2).

the same experiment (Fig. 5II). As already pointed out, N_2 production begins only when NO starts to be desorbed into the gas phase. Moreover, the maximum desorption rates for both gases are coincident. Therefore the reaction between NO (or NO_2) and adsorbed NH_3 follows an Eley–Rideal mechanism on the CCCM-Mn catalyst.

It is somewhat surprising that the NO released during the NH_3 stage (Fig. 5I) does not produce N_2 via further reaction with adsorbed NH_3, as does the NO released during the TPD. This is because the nitrogen oxides released during the TPD are mainly NO_2 (from nitrate decomposition) whereas the nitrogen oxides observed during the passage of NH_3 correspond to the NO produced by the desorption of bridged nitrites. As noted before, gaseous NO reacts with preadsorbed NH_3 to give N_2. However, at 125 °C this reaction is very slow, as can be deduced from the slow decay of N_2 during the passage of NO (curve g in Fig. 3). It can be assumed therefore that the NO escaping from the catalyst surface has no time to react with the adsorbed NH_3, and is unable to produce N_2.

On the other hand, the decomposition of surface nitrates during the TPD produces mainly NO_2, although this gas is detected as NO due to its transient release. The NO_2 molecules are able to react with the adsorbed NH_3 when escaping from the surface, especially with the ammonia species ascribed to the MT and HT peaks of the NH_3-TPD, whose maximum desorption temperatures (262 and 370 °C, respectively; Table 1) are above that for the HT peak of the NO-TPD (231 °C). As can be seen in Fig. 3 the production rate of N_2 when NO + O_2 is introduced into the system after the adsorption of NH_3 (curve k) is much faster than that observed when only NO is passed through the catalyst. This can be attributed to a faster SCR reaction by NO_2 which is produced by reaction (7). It can, therefore, be concluded that NO_2 is more reactive than NO toward the SCR reaction and consequently can partly react with the adsorbed NH_3 species when it is formed by nitrate decomposition during the TPD stage.

Finally, the fact that the incoming NH_3 causes the release of bridged nitrites from the catalyst surface explains the peculiar evolution of this surface species during the SCR process (codes d1 to d5 in Table 2), a matter that was left unexplained in [11]. As can be seen, the initial increase in the amount of surface nitrites is produced when the catalyst surface is far from being saturated with weakly adsorbed NH_3 (points d1 to d3 in Fig. 4). When the surface starts to be saturated with weakly adsorbed NH_3 (points d4 and d5 in Fig. 4), the nitrites are displaced from the surface (codes d4 and d5 in Table 2). As happened with the surface nitrites formed on the carbonaceous surface by the carbon-catalyzed oxidation of NH_3, the nitrites formed on the manganese oxide start to be displaced by NH_3 only when the NO-free sites have already been occupied by NH_3. In this process the possibility of a spillover phenomenon cannot be disregarded. This transient reaction can be written as:

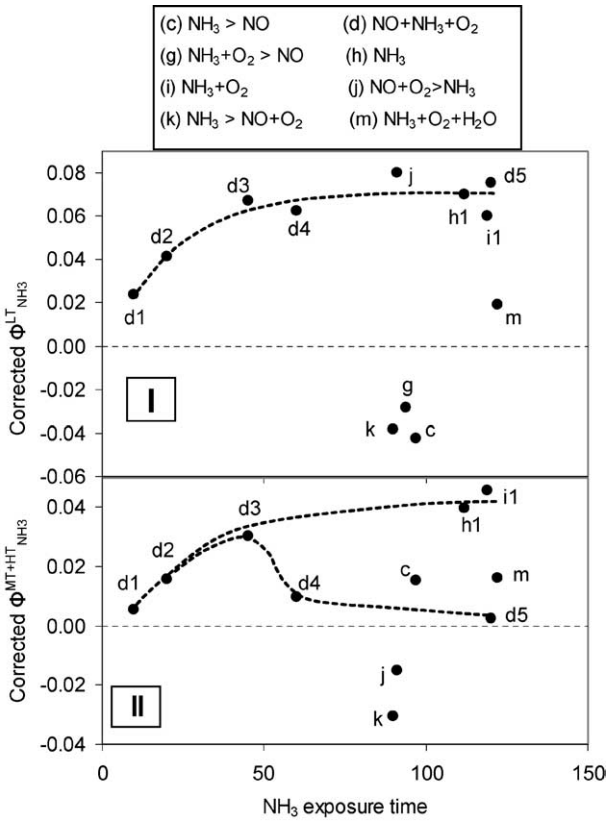

Fig. 6. Moles of desorbed NH_3 per manganese moles (corrected for support desorption) versus NH_3 exposure time for: (I) LT peak of the NH_3-TPD, (II) MT + HT peaks of the NH_3-TPD. The legends indicate the corresponding step-response sequences at 125 °C performed over CCCM-Mn (codes as in Table 3).

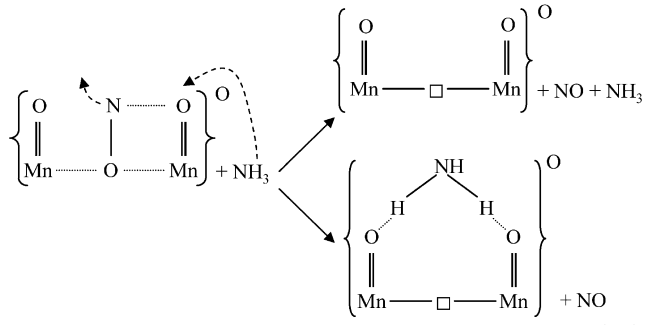

(12)

At this stage it is not possible to discriminate between the options suggested by reaction (12), although considering the minute contribution of (12) to the SCR process as a whole, this point is of minor importance. A similar reaction can be established for the competition of water with surface nitrites (point f in Table 2), by merely substituting H_2O for NH_3 in reaction (12).

4.2.4. NH_3 desorbed in the low-temperature peak ($\Phi^{LT}_{NH_3}$): steady-state SCR

Fig. 6I plots the experimental corrected values of $\Phi^{LT}_{NH_3}$ vs the NH_3 exposure time for all the experiments performed

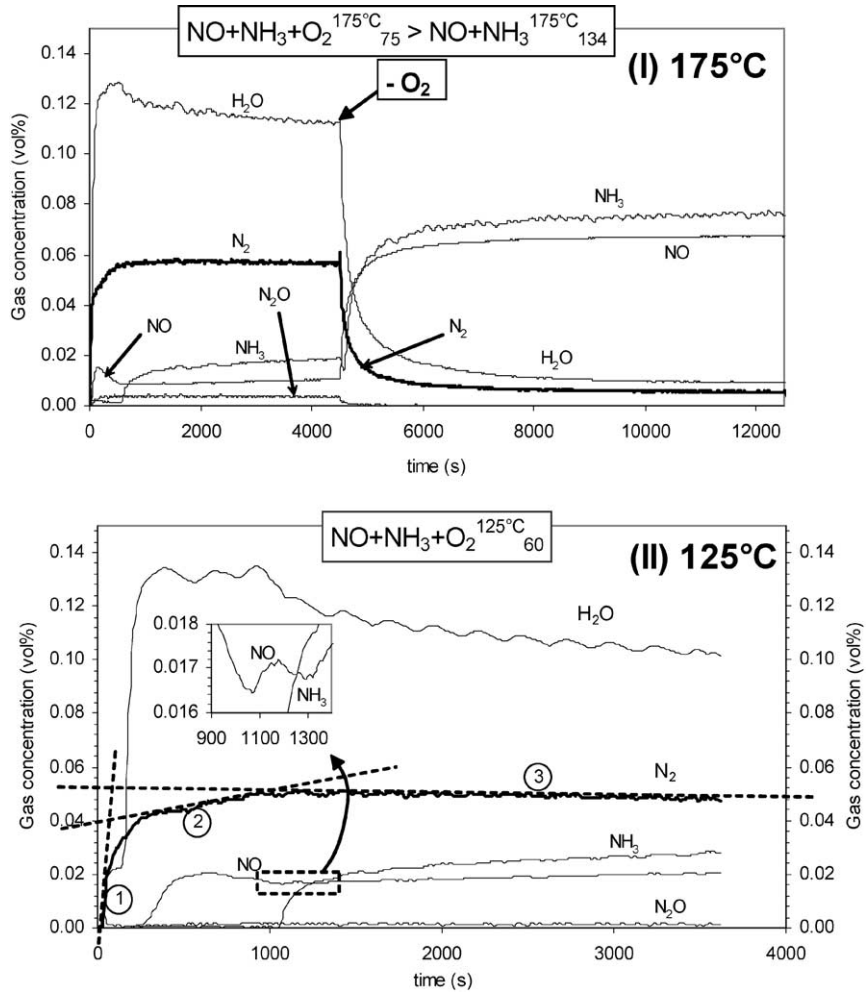

Fig. 7. Evolution of gas-phase composition during the step-response stage of the SCR experiments indicated in the figure: (I) 175 °C, (II) 125 °C.

with NH_3. Negative values imply that the NH_3 species ascribed to the LT peak has been removed not only from the active phase but also from the carbonaceous support. As observed, the presence of water (point m) causes a decrease in the LT peak area. This can be attributed to the fact that the NH_3 species ascribed to the LT peak originates from the previously weakly adsorbed NH_3. This species must fulfill the following requisites: (i) it must be formed without the participation of gas-phase oxygen (which explains the similarity of the corrected $\Phi^{LT}_{NH_3}$ values for the $NH_3{}^{125\,°C}$ and $NH_3 + O_2{}^{125\,°C}$ experiments (points h1 and i1 in Fig. 6I)); and (ii) it must not occupy oxygen vacancies on the manganese oxide, so that it does not compete with adsorbed nitrosyls. These two premises are accomplished by the oxyamine species formed via the following equilibrium:

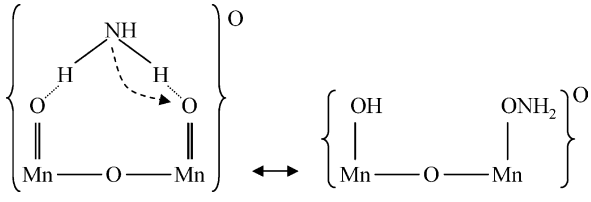

(13)

Several authors have proposed that the adsorption of NH_3 over a vanadium-based catalyst leads to the formation of the intermediate aminooxy groups, V–ONH_2 [18,22,23,30,31]. In a recent work provided by Larrubia et al. [32] it was stated that the spectroscopic features of adsorbed hydroxylamine (oxyamine is a dissociated form of hydroxylamine) are hardly distinguishable from those of coordinated ammonia, so that spectroscopic confirmation or rejection of the –ONH_2 species is not straightforward. According to Kapteijn et al. [5], coordinated ammonia species present symmetric deformation in the 1100–1320 cm^{-1} region and some of the peaks observed in the infrared spectra displayed in a previous work [11] for CCCM-Mn subjected to SCR reaction are located in this spectral region. We can therefore assume that the bands at 805, 1097, and 1263 cm^{-1}, as displayed in Fig. 7 of [11], are produced by the vibrations of aminooxy groups.

As noted in the previous sections, the ammonia species ascribed to the LT peak (aminooxy groups) react with NO in the SCR process at 125 °C, which is consistent with the position of points k, g, and c in Fig. 6I. However, under pseudo-steady-state conditions ($t > 60$ min) the corrected

area of the LT peak is very similar both in the presence and in the absence of NO (points j, i1, h1, and d5 in Fig. 6I). Two interesting conclusions can be drawn from this:

1. Under the TPD conditions, gas-phase NO_2 reacts with the NH_3 species ascribed to the MT and HT peaks, but not with the NH_3 species ascribed to the LT peak, at least not fast enough for the fugitive NO_2 molecules. This is deduced by comparing the TPD areas of the experiments in which NO_2 does not evolve during the TPD (points h1 and i1 in Fig. 6I and Table 3) and those of the experiment in which NO_2 is released during the TPD (point j in Fig. 6I and Table 3). However, as can be seen from Fig. 3, when NO and O_2 are continuously supplied, the NO_2 formed must react with $–ONH_2$; otherwise the long and gradual decay for times above 1000 s exhibited by the curves in which only NO is supplied after NH_3 (curves c and g) would also be appreciated for the curve in which $NO + O_2$ is supplied (curve k). It can be concluded that reaction of NO_2 with the $–ONH_2$ groups (LT peak) is slower than the reaction of NO_2 with the NH_3 species ascribed to the MT and HT peaks. The last sector of curve k (slope between ~ 300 and ~ 1200 s) corresponds, therefore, to the reaction of NO and NO_2 with the $–ONH_2$ groups. Thus, the acute N_2 release peak displayed by curve k in Fig. 3 is formed by the combined contribution of the N_2 produced by the reaction of NO_2 with the species ascribed to the MT and HT peaks and the N_2 that results from NO reduction on the oxygen vacancies. The overlapping of both contributions can be detected in the circled sector of curve k in Fig. 3.
2. The reactions of NO/NO_2 with $–ONH_2$ are significantly slower than the aminooxy formation reaction (13). Equilibrium (13) is attained rapidly as can be deduced from the roughly constant values of the $\Phi^{LT}_{NH_3}/\Phi^{iso}_{NH_3}$ ratio (corrected values) in the absence of water: 1 ± 0.2. This value therefore must be the equilibrium constant of reaction (13) at 125 °C.

Aminooxy groups are known to react under ambient conditions with ketones and aldehydes to form stable oximes. This reaction has recently been used in the immobilization of polymers and nanoclusters [33,34] and can be schematized as follows:

$$R–O–NH_2 + O{=}CH–R' \rightarrow R–O–N{=}CH–R' + H_2O. \quad (14)$$

Similarly we propose the following reaction paths for the reduction of NO and NO_2 with the aminooxy groups formed on the manganese oxide, by substituting R′–CH=O for NO or NO_2 in (14), and allowing the subsequent desorption of N_2:

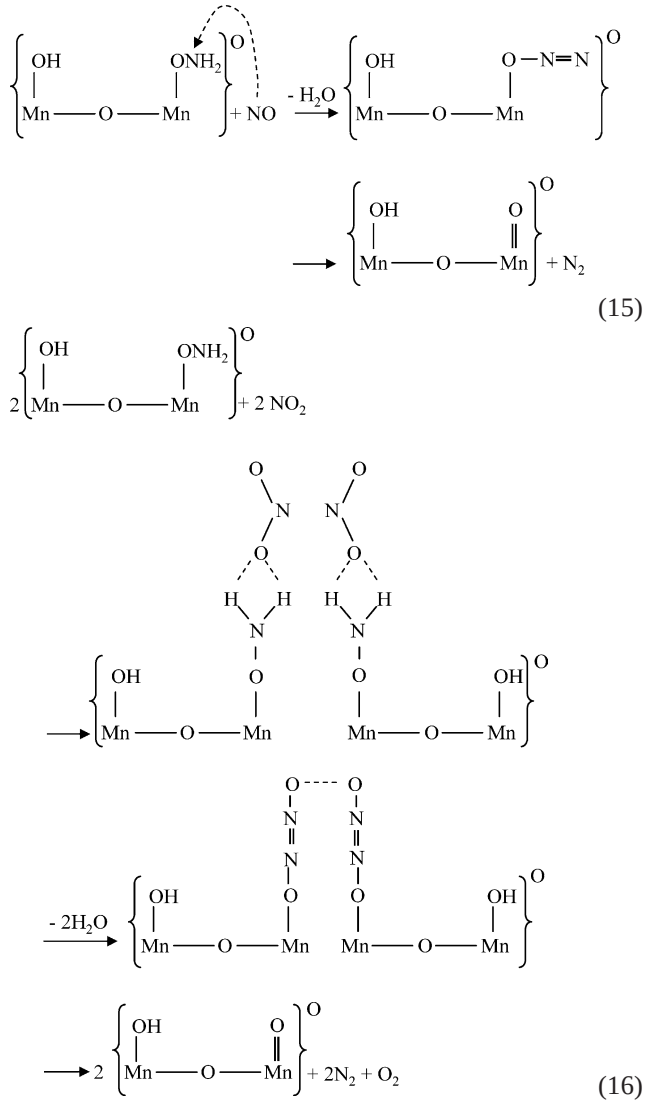

At 125 °C reaction (16) is faster than reaction (15), although both are slow enough to ensure the saturation of the oxide with aminooxy groups in the steady state. The desorption of small amounts of N_2 and O_2 was observed during the isothermal desorption stage of the $NO + O_2 + NH_3$ $^{125\,°C}$ experiments performed after the reaction stage. This is consistent with the mechanism proposed for reaction (16).

At this point we can try to interpret the transient processes that produce the trends depicted in Fig. 3 in the light of the reactions proposed for N_2 formation. In the NH_3 presaturated samples (curves c, g, and k), when only a small fraction of oxygen vacancies is available on the manganese oxide (curve c), direct reaction on the vacancies cannot initially reduce all the incoming NO and so reaction (15) starts at $t = 0$. This explains the differences between curves a2 (where the reaction only occurs on vacancies) and c (where the reaction on vacancies and the reaction (15) overlap). On the other hand, when a large amount of vacancies is available due to previous or simultaneous reduction via evolving CO (curves g and k), two situations arise:

1. In the absence of O_2 (curve g) all incoming NO is initially reduced on the oxygen vacancies and reaction (15) starts to acquire relevance when NO becomes available due to the progressive filling of the oxygen vacancies. This is deduced from the shape of the curve of water release (inset) whose maximum rate is clearly displaced at $t > 0$, and from the appearance of a second peak in the curve of N_2 release, corresponding to the onset of N_2 desorption formed via reaction (15). The fact that this peak is slightly displaced with respect to the water release peak suggests that N_2 desorption in reaction (15) is not an instantaneous process.
2. In the presence of oxygen (curve k) there is no apparent restriction for the simultaneous occurrence of NO reduction on the oxygen vacancies or for NO_2 formation via nitrosyl oxidation, so that the SCR reactions of NO_2 with the adsorbed NH_3 species (LT (16) and MT + HT peaks) occur from the very beginning of the step, as does the direct reaction of NO with the aminooxy groups (15), though the latter takes place to a lesser extent. This overlapping explains the difference in the values of maximum rate of N_2 release for curves k (with preadsorbed NH_3) and b2 (without preadsorbed NH_3).

In the light of the facts presented above, the initial values for reactions (15) and (16) at 125 °C can be estimated by extrapolating to $t = 0$ the straight sections of curves c and k, respectively, within a time interval in which NO reduction on the vacancies (and SCR reaction of MT + HT peaks) is minimal (i.e. ∼ 700–1000 s). This procedure yields the values displayed in Table 5, which are $\sim 5.0 \times 10^{-5}$ and $\sim 2.1 \times 10^{-4}$ $mol_{N_2}\ mol^{-1}{}_{Mn}\ s^{-1}$) for (15) and (15) + (16), respectively, indicating that at 125 °C NO_2 reduction by the aminooxy groups is about 3 times faster than NO reduction by the same groups.

In a previous work [11] it was suggested that the enhanced formation of nitrosyls and nitrites under the SCR conditions for low NO exposure times could be due to an increase in the creation of oxygen vacancies resulting from the SCR mechanism itself. This can be clearly seen in the $NH_3{}^{125\,°C} > NO + O_2{}^{125\,°C}$ experiment (point k in Table 2), in which the amounts of nitrosyls (Φ_{NO}^{iso}), nitrites (Φ_{NO}^{LT}), and nitrates (Φ_{NO}^{HT}) are remarkably high. The formation of these species is favored by the presence of oxygen vacancies ((3) and (6)–(8)). However, for this experiment the excess of surface NO species cannot be explained solely by the O_2-related creation of oxygen vacancies, which would induce an adsorption of NO species lower than the one observed (see $NO + O_2{}^{125\,°C}$ experiments: points b in Table 2), nor by the previous NH_3 step, in which the passage of NH_3 by itself is not able to produce oxygen vacancies, as discussed above. Consequently, the oxygen vacancies on the manganese oxides must be caused by certain reactions of the SCR mechanism. Reactions (15) and (16) do not produce vacancies and so these must be formed in a subsequent stage.

In the light of these considerations we propose that the vacancies are formed by surface dehydroxylation of the solid product of reactions (15) and (16):

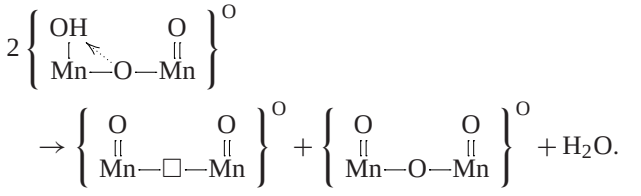

(17)

This step is a necessary part of most SCR mechanisms, as reported by Busca et al. [27]. The special characteristic proposed for reaction (17) is that one labile oxygen atom of the octahedral phase removes two hydrogen atoms from the adjacent hydroxyl groups. The dehydrogenation activity of surface oxygen in the Mn_3O_4 catalyst has already been studied by Baldi et al. [1] in the process of propane oxydehydrogenation. Other possible paths should also take into account the stoichiometry of reaction (17), the only restriction being that gaseous oxygen cannot participate directly in the reaction, at least at 125 °C, as, at this temperature, O_2 does not dissociate on the vacancies.

In order to close the redox cycle and retain catalytic activity in the steady state, the oxygen vacancies created by reaction (17) must be refilled, or in other words, the octahedral phase of the manganese oxide must be reoxidized. Two situations can be encountered:

1. *In the absence of gas-phase oxygen* there is steady-state conversion of NO to N_2 as observed in Fig. 7I. Thus, for the experiment depicted in the figure ($NO + O_2 + NH_3{}^{175\,°C}{}_{75} > NO + NH_3{}^{175\,°C}{}_{134}$) the values of steady-state conversion of NO to N_2 were ∼ 84% for the first step and ∼ 9% for the second step. The steady-state level of water in the second step confirms the view that the residual conversion of NO to N_2 is a product of reaction (15). In this situation there is only one way to ensure the reoxidation of the manganese oxide so that the catalytic cycle can be closed: the reduction of nitrosyls on oxygen vacancies ((3) + (4)). In principle this should be a rapid (noncontrolling) process, as can be seen from the acute N_2 peaks observed in Fig. 3. In fact, the value for the N_2 formation rate in the absence of oxygen evaluated at the steady state for the $NO + O_2 + NH_3{}^{175\,°C}{}_{75} > NO + NH_3{}^{175\,°C}{}_{134}$ experiment is 7.1×10^{-5} $mol_{N_2}\ mol^{-1}_{Mn}\ s^{-1}$ (Table 5), a value that might well correspond to the reaction rate of (15) at 175 °C, since at 125 °C this was estimated to be $5.0 \times 10^{-5} mol_{N_2}\ mol^{-1}_{Mn}\ s^{-1}$ (Table 5). All of these arguments imply that the controlling step of the whole process is the SCR reaction (15). This is further supported by the high rate of the dehydroxylation reaction, which is implied by the large amount of nitrosyls and bridged nitrites on the catalyst surface for very low reaction times (code d1 in Table 2).

Table 5
Values estimated for different reaction rates

Experiment	State	Reaction[b]	T (°C)	Rate ($mol_{N_2}\ mol_{Mn}^{-1}\ s^{-1}$)
$NH_3{}^{125\,°C}{}_{97} > NO^{125\,°C}{}_{94}$	Transient[a]	$(15)^O$	125	5.0×10^{-5}
$NH_3{}^{125\,°C}{}_{90} > NO + O_2{}^{125\,°C}{}_{100}$	Transient[a]	$((15)+(16))^O$	125	2.1×10^{-4}
$NO + NH_3 + O_2{}^{125\,°C}{}_{120}$	Pseudo-steady state	$((15)+(16))^O + (23)^T$	125	5.4×10^{-4} (30 min) 4.6×10^{-4} (120 min)
$NO + O_2 + NH_3{}^{175\,°C}{}_{75} > NO + NH_3{}^{175\,°C}{}_{134}$	Steady state	$(15)^O$	175	7.1×10^{-5}
$NO + O_2 + NH_3{}^{175\,°C}{}_{75} > NO + NH_3{}^{175\,°C}{}_{134}$	Pseudo-steady state	$((15)+(16))^O + (23)^T$	175	7.3×10^{-4} (30 min) 7.2×10^{-4} (75 min)

[a] Initial rate evaluated by the extrapolation of interval 700–1000 s.
[b] Superscripts indicate the manganese oxide phase in which reactions occur (O, octahedral; T, tetrahedral).

Summing up, in the absence of oxygen, the steady-state SCR mechanism at 125 °C on the octahedral phase of the manganese oxides comprises the following steps: (i) NH_3 adsorption on the oxygen atoms, which partly competes with the preadsorbed water molecules (9), (ii) formation of the aminooxy groups (13), (iii) SCR reaction of these groups with gas-phase NO (15), (iv) surface dehydroxylation (17), and (v) surface reoxidation of oxygen vacancies via nitrosyl reduction to N_2 ((3) + (4)). The controlling step of the whole process is the SCR reaction (15) itself (step (iii)).

In the absence of an SCR reaction, water is released mainly in the initial transient period from the catalyst surface (i.e., during a single NH_3 passage; Fig. 2I). In contrast, the SCR reaction causes the continuous release of water in the steady state, as observed in Figs. 7I and 7II, where the evolution of water under SCR conditions at 125 and 175 °C is displayed. As noted previously, some of this water may be adsorbed on the oxygen atoms of the manganese oxides via the following equilibrium:

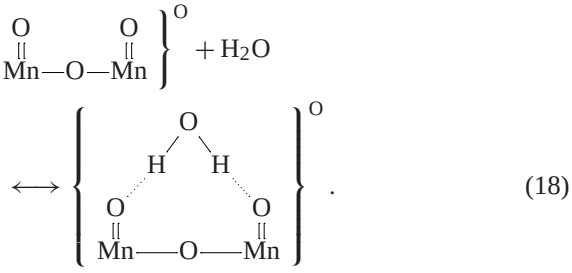

(18)

Now, all the reactions needed to close the catalytic cycle in the absence of oxygen on the octahedral phase of the manganese oxides have been defined. This cycle is depicted in Fig. 8I in which the appropriate combination of reactions is included. This cycle yields the expected SCR stoichiometry in the absence of oxygen [27]:

$$6NO + 4NH_3 \rightarrow 5N_2 + 6H_2O. \quad (19)$$

2. *In the presence of gas-phase oxygen* other facts must be considered. As oxygen cannot reoxidize the generated vacancies at 125 °C, reoxidation of the active phase must be performed by a different agent. The difference with respect to the reaction in the absence of oxygen is that now we have two possible oxidants: NO and NO_2. The latter is known to be a more active oxidant than NO and O_2 [35]. If NO_2 oxidizes the oxygen vacancies, then oxygen acts as a reagent in the SCR process on the octahedral Mn_3O_4 phase. On the other hand, if NO is responsible for closing the redox cycle, then gas-phase oxygen is in fact acting as a catalyst, since the same amount of oxygen that produces NO_2 (reaction (7) is afterward released during the SCR reaction (6) (this is not completely true since the formation of surface nitrates consumes oxygen, though at a very slow rate). Under these conditions the SCR reaction would progress according to Eq. (19). In principle it is difficult to make a definite decision on this issue, on the basis of the results available. One possible way to solve the problem is to assess the ratio of consumed NH_3 per consumed NO during the SCR reaction. The value of this ratio is 0.67 in the absence of oxygen (reaction (19)) and 1.00 for the classical SCR reaction in the presence of oxygen [27]:

$$4NO + 4NH_3 + O_2 \rightarrow 4N_2 + 6H_2O. \quad (20)$$

Considering all the possible sinks and sources of NO and NH_3 (SCR plus side reactions as NH_3 oxidation (Table 4)), the experiment displayed in Fig. 7II yields a ratio of gas consumption via the SCR reaction (NH_3/NO) of 0.82, which is somewhere between the values corresponding to reactions (19) and (20). As will be discussed in the following section, the SCR reaction on the tetrahedral environment of the manganese oxide initially accounts for about half of the N_2 produced at 125 °C and operates according to reaction (20). This suggests strongly that the SCR reaction on the octahedral environment is responsible for decreasing the NH_3/NO consumption ratio from 1.00 to 0.82. In this case it progresses according to (19). In other words, even in the presence of oxygen at 125 °C NO performs the oxidation step needed to close the catalytic cycle.

With this, the set of reactions for the SCR mechanism at 125 °C on the octahedral phase of the manganese oxides is completed. Again, in the presence of O_2 the controlling step is the SCR reaction (16). This is indicated by

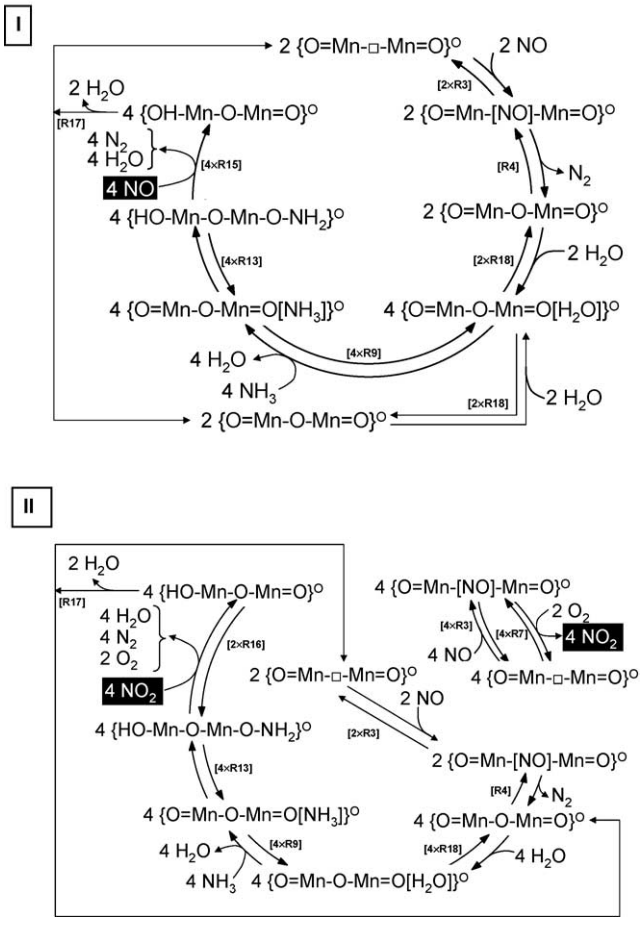

Fig. 8. Mechanism of the steady-state SCR reaction: (I) in the absence of oxygen; (II) in the presence of oxygen.

the low availability of oxygen vacancies in the steady state (low value of Φ_{NO}^{iso} at high NO exposure times; Table 2), which implies a comparatively high rate for the oxidizing reaction (in principle (3) + (4)).

To summarize, in the presence of oxygen, the steady-state SCR mechanism at 125 °C on the octahedral phase of the manganese oxides, plotted in Fig. 8II comprises the following steps: (i) NH_3 adsorption on the oxygen atoms, which partly competes with the preadsorbed water molecules (9), (ii) formation of the aminooxy groups (13), (iii) NO adsorption as nitrosyls on the oxygen vacancies (3), (iv) oxidation of the surface nitrosyls to gas-phase NO_2 (7), (v) SCR reaction of aminooxy groups with gas-phase NO_2 (16), (vi) surface dehydroxylation (17), and (vii) surface reoxidation of oxygen vacancies via nitrosyl reduction to N_2 ((3) + (4)). The controlling step of the whole process is the SCR reaction (16) itself (step (v)). It can be seen that the appropriate combination of reactions yields the SCR stoichiometry for reaction (19).

In principle the proposed mechanisms are thought to occur at a steady rate during the SCR process. As will be discussed below, the slow deactivation of the catalyst is related to the $NO/NH_3/O_2$ interactions that occur in the tetrahedral phase of the catalyst.

4.2.5. NH_3 desorbed at the medium and high-temperature peaks ($\Phi_{NH_3}^{MT+HT}$): pseudo-steady-state SCR mechanism

The reaction rates values obtained for (15) and (16) at 125 °C (5.0×10^{-5} and 1.6×10^{-4} $mol_{N_2}\, mol_{Mn}^{-1}\, s^{-1}$, respectively; Table 5) cannot explain the high nitrogen formation rate observed under the SCR reactions. This can be calculated at the pseudo-steady state from the slope of the dashed line associated with sector 3 of the N_2 evolution curve during SCR at 125 °C (Fig. 7II). The values of the rate vary from 5.4×10^{-4} $mol_{N_2}\, mol_{Mn}^{-1}\, s^{-1}$ at 30 min to 4.6×10^{-4} $mol_{N_2}\, mol_{Mn}^{-1}\, s^{-1}$ at 120 min. This means that a process different to reactions (15) and (16) yields about 60% of the total N_2 produced, this proportion decreasing gradually with time to a point where it disappears altogether. From the results analyzed in previous sections it can be concluded that this process consists of an SCR reaction of NO_2 with the NH_3 species ascribed to the MT and HT peaks. These species, as previously pointed out, are ammonium ions formed on the hydroxyl groups that were produced by reaction (2) on the tetrahedral phase of the manganese oxides. The presence of NH_4^+ ions on the Brønsted sites of the metal oxide surfaces is typically detected by asymmetric bending vibrations in the 1400–1500 cm^{-1} region (V_2O_5/TiO_2, 1428 cm^{-1} [36]; Mn_2O_3, 1459 cm^{-1} [9]; Fe-MOR, 1463 cm^{-1} [37]; Fe-ZSM5, 1473 cm^{-1} [38]; MnO_x/Al_2O_3, 1480 cm^{-1} [5]; etc). Kapteijn et al. [5] also report a vibration band at 1390 cm^{-1} for NH_4^+ on MnO_x/Al_2O_3. The infrared results displayed in [11] neither confirm nor refute the presence of NH_4^+ on the surface of the catalyst after the SCR reaction at 175 °C. However, emerging through the noise of the IR signal there appears to be a conspicuous band at 1407 cm^{-1} which could be assigned to NH_4^+ ions.

Fig. 6II offers the variations with NH_3 exposure time of the corrected area values for the combined contribution of the MT and HT peaks to the NH_3-TPD. The MT and HT peaks were analyzed as a whole and not separately due to the close relation between the areas of both peaks (the corrected Φ values follow the general trend $\Phi_{NH_3}^{HT} = 0.41\Phi_{NH_3}^{MT}$; $R^2 \approx 0.8$). These values suggest that similar processes are involved in the formation of the species responsible for both peaks. For the experiments in which NO and NH_3 species were present on the surface of the catalyst prior to the TPD stage (c, d, j, k, in Fig. 6II), the normalized amount of N_2 released during the TPD was added to the $\Phi_{NH_3}^{MT+HT}$ values (open symbols). As already noted this N_2 comes mainly from the SCR reaction of evolving NO_2 with the NH_3 species of the MT and HT peaks.

As can be seen in the figure, when NO is passed through the catalyst after NH_3 adsorption there is only a small decrease in the value of $\Phi_{NH_3}^{MT+HT}$ (point c), as compared to the large decrease caused by the passage of NO + O_2 (point k).

This is an indication of a higher rate of reaction of NO_2 with the related NH_3 species compared to that of NO.

Under SCR conditions (points d in Fig. 6II), the values of $\Phi_{NH_3}^{MT+HT}$ initially increase up to approximately the maximum possible value, and then start to decrease slowly. The initial increase of the $\Phi_{NH_3}^{MT+HT}$ values with NH_3 exposure time is parallel to that of $\Phi_{NH_3}^{iso}$. This suggests that the MT-HT peak species are formed by the surface migration of weakly adsorbed NH_3. The decrease of $\Phi_{NH_3}^{MT+HT}$ caused by the presence of water (point i1 vs point m) is consistent with this assumption. On the other hand, the slow decrease of $\Phi_{NH_3}^{MT+HT}$ after they have reached the maximum value is parallel to the decrease observed for the overall reaction rate (Fig. 7II) and to the increasing trend in the amount of nitrates adsorbed on the tetrahedral phase of the manganese oxides (Φ_{NO}^{HT} in Table 2).

To recapitulate: (i) the reaction of NO_2 with the NH_3 species ascribed to the MT and HT peaks is faster than reactions (15) or (16), (ii) the temperature range of the desorption of the MT and HT peaks is similar to that of ammonium ions adsorbed on the acid hydroxyl groups of zeolites, (iii) under SCR conditions the decreasing trend of the $\Phi_{NH_3}^{MT+HT}$ values (Fig. 6II) is parallel to the decreasing rate of N_2 formation (stage 3 in Fig. 7II) and to the increasing amount of nitrates adsorbed on the tetrahedral phase of the manganese oxides (Φ_{NO}^{HT} in Table 2).

All of these results point to a singular mechanism in which two types of ammonium ions of different strength (thereby producing MT and HT peaks) bonded to the hydroxyls of the tetrahedral phase of the manganese oxide react mainly with NO_2 (more slowly with NO) to produce N_2. In the presence of $NO + O_2$ the availability of ammonium ions decreases with time due to the gradual formation of nitrates. The following reactions for the formation of NH_4^+ ions are therefore proposed:

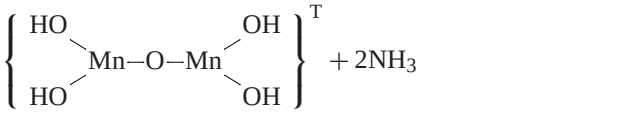

$$\rightarrow$$

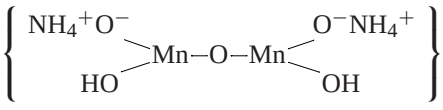

(21)

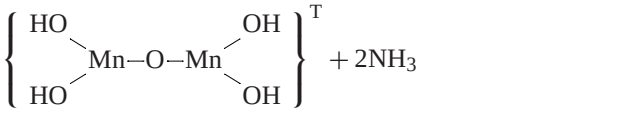

$$\rightarrow$$

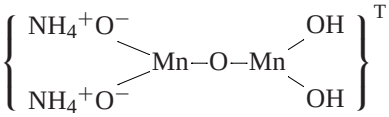

(22)

Of course these reactions are proposed only as an attempt to explain the different thermal desorption ranges of the MT and HT peaks. In any case, the general concept of ammonium formation on the hydroxyl groups can be accepted from the conclusions of the results discussed. These reactions only occur on the manganese atoms associated with the oxygen excess x ($Mn_3O_{4+0.5x}$). Assuming that at 125 °C all the available hydroxyls adsorb NH_3 molecules according to the stoichiometry of reactions (21) or (22), the oxygen excess can be roughly calculated as $x = 3\Phi_{NH_3}^{MT+HT}$. For the maximum value of $\Phi_{NH_3}^{MT+HT}$ (~ 0.05) oxygen excess adopts a value of $x \approx 0.15$, which is well within logical expectations ($0 < x < 1$).

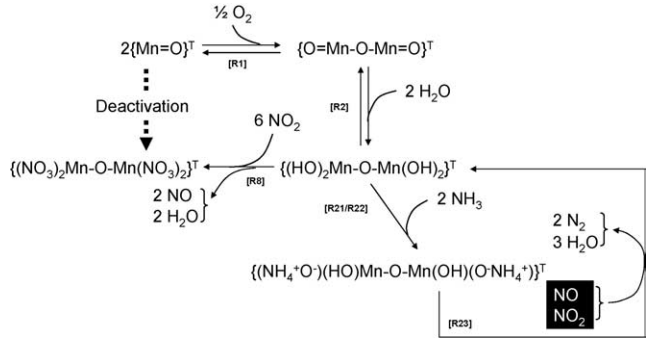

Fig. 9. Deactivation mechanism of the tetrahedral phase of the manganese oxides.

The reaction of NO_2 with ammonium ions on a solid surface is commonly used in the preparation of solid oxides. With respect to the SCR process, this reaction has been thoroughly studied by the group of Long and Yang [37–39] with iron-exchanged zeolites, with the result that the reaction rate with $NO + O_2$ was much higher than with only NO, which is in agreement with the results obtained in the present work. We should therefore be able to apply the same reaction mechanism for our catalytic system:

$$\{(NH_4{}^+O^-)(HO)Mn\text{–}O\text{–}Mn(OH)(O^-NH_4{}^+)\}^T + NO + NO_2 \rightarrow \{(HO)_2Mn\text{–}O\text{–}Mn(OH)_2\}^T + 2N_2 + 3H_2O. \quad (23)$$

As expected, the appropriate combination of reactions ((3) + (7) + (21)/(22) + (23)) yields reaction (20) for the whole SCR process on the tetrahedral phase of the manganese oxides.

The gradual deactivation of reaction (23) occurs through the substitution of the hydroxyl groups for nitrates (reaction (8)). This reaction competes with the SCR reaction, as indicated in Fig. 9. Initially the active phase has an arbitrary solid concentration of tetrahedral MnO. At 125 °C this is in equilibrium with a given concentration of the product of reaction (1) (oxygen excess formation) which depends on its equilibrium constant [20]. In the absence of (8), oxidized MnO ('oxygen excess') would continue to react through (2), (21)/(22), and (23) in a steady SCR cycle. The role of reaction (8) is to remove hydroxyl groups by the formation of nitrates. It therefore acts as a sink for oxidized Mn=O. Reaction (8) causes the progressive decrease of the $\{Mn{=}O\}^T$ concentration by shifting equilibria (1) and (2) to the right. This is reflected in the loss of activity of the tetrahedral phase. Ideally, in the steady state the whole $\{Mn{=}O\}^T$ phase should have been converted to manganese

nitrates. However, under SCR conditions the nitrate formation rate is rather low (see Φ_{NO}^{HT} evolution for points d1–d5 in Table 2) as a consequence of the diminished availability of NO_2 (reactions (16) and (23)) and hydroxyl groups (reaction (21)/(22)) and so the deactivation progress is very slow, hence the label *pseudo-steady state*. In fact, a comparison of the reaction rates of ((15) + (16)) at 125 °C with that of ((15) + (16) + (23)) (Table 5) the rate for (23) should become zero (complete deactivation) at ∼ 6 h; from this point, the residual catalytic activity at steady state would be due to reactions (15) and (16), though mainly the latter.

Reaction (1) implies that oxygen can cause a slight oxidation of the tetrahedral MnO phase at 125 °C. This is consistent with the stability of tetrahedral Mn^{3+}–O bonds associated with the oxygen excess, which was found to be higher than that corresponding to the octahedral long Mn^{3+}–O bonds, the latter being responsible for the formation of oxygen vacancies. Reaction (1) does not, therefore, contradict the fact that oxygen does not dissociate on the octahedral vacancies at 125 °C.

We can now interpret the transient behavior of the different gases during the SCR reaction at 125 °C (Fig. 7II). During the first stage (1), N_2 evolution is rapid as a consequence of NO reduction on the oxygen vacancies, their number being significantly increased by the presence of oxygen which gives rise to the evolution of CO [11]. The small H_2O step (∼ 0.02%) observed at this stage is mainly due to the release of H_2O from the oxidation of the support [11]. During stage (2) N_2 evolves mainly through combined SCR reactions. The steady increase in the concentration of N_2 is a consequence of the increased availability of surface aminooxy groups (Fig. 6I) and ammonium ions (Fig. 6II). At this stage H_2O release is significantly increased by the combination of a variety of factors: (i) the SCR reactions ((15) + (16) + (23)), (ii) the displacement of H_2O by weakly adsorbed NH_3 (9), and (iii) H_2O released as a consequence of nitrate formation (8). The maximum of NO concentration observed at this stage is a consequence of the intersection between the decreasing rate of NO reduction by oxygen vacancies (curve b2 in Fig. 3) and the increasing rate of NO reduction via SCR reactions as a consequence of the increased availability of surface ammonia-derived species. Finally, in stage (3) the concentration of H_2O starts to decrease for two reasons: (i) the reduced availability of weakly adsorbed water for reaction (9), and (ii) the decreased SCR reaction rate of NO_2 with ammonium ions (23) due to the progressive deactivation of the tetrahedral phase (8). The second reason also explains the increasing trend of the NH_3 and NO concentrations and the decreasing trend of N_2. Surface nitrites formed by reaction (6) are released at the beginning of this stage (reaction (12); Φ_{NO}^{LT} in Table 2). This phenomenon is hardly noticeable in Fig. 7II since its contribution to total NO release is very small (Fig. 5I), but it can be appreciated in the enlarged section displayed in the inset. To conclude, the small amount of N_2O detected in the gas phase during the whole process is due to the oxidation of weakly adsorbed NH_3 (11).

4.2.6. Temperature-based transition toward a more conventional mechanism

Although this work has mainly focused on the SCR mechanism at a low temperature (125 °C), the information obtained from the experiments performed at a higher temperature (175 °C) also gives rise to some interesting conclusions. At 175 °C oxygen can be dissociated on the oxygen vacancies of the manganese oxides. At the same time NO_2 formation starts to be hampered by thermodynamic constrictions. This explains the inverse relationship between the concentration of surface nitrates and temperature (the value of Φ_{NO}^{HT} decreases from ∼ 0.2 at 125 °C to ∼ 0.1 at 175 °C (Table 2)). The increased temperature favors the oxidation of the tetrahedral phase via gas-phase oxygen, as can be seen from the greater increase of the $\Phi_{NH_3}^{MT+HT}$ value when oxygen is added to the gas phase (codes 13 and 14 in Table 3: from ∼ 0.03 to ∼ 0.09). At 125 °C this increase is much smaller (codes h1 and i1 in Table 3: from ∼ 0.06 to ∼ 0.08).

Thus there is a transition stage in which all the mechanisms discussed for the reaction at 125 °C start to evolve toward a limiting mechanism in which: (i) NO replaces NO_2 (no longer formed) as the main reagent in the SCR reaction, (ii) the reoxidation of the active phase is performed by gas-phase oxygen instead of NO/O_2, (iii) nitrate formation does not take place since NO_2 is no longer available. This is consistent with the conventional SCR mechanisms reported in most of the literature. However, this discussion is irrelevant for the system studied in this work, since a higher temperature also implies extensive oxidation of the carbonaceous support [6,7] and consumption of NH_3 in unwanted oxidation reactions (10) and (11).

5. Conclusions

This report analyzes the role of surface NH_3 species in the low-temperature (125 °C) SCR mechanism with the aim of determining the mechanism of the SCR reaction in this catalyst. The following conclusions can be drawn from what has been discussed:

NH_3 is weakly adsorbed on oxygen atoms of both the carbonaceous support and the active phase. Ammonia adsorbed by the support at 125 °C (∼ 30% of total adsorbed ammonia) produces an insignificant amount of NO by reacting with gas-phase oxygen. The rest of the weakly adsorbed ammonia is linked via hydrogen bonds to the oxygen atoms of the octahedral phase of Mn_3O_4. This adsorption displaces water and the not very significant linear (monodentate) or bridged nitrites previously present on the same oxygen atoms. In the presence of oxygen a small quantity of the ammonia weakly adsorbed by the active phase is converted to N_2 and N_2O. Weakly adsorbed ammonia is partly converted to aminooxy groups by reaction with lattice oxy-

gen. The aminooxy groups are an active species in the SCR reaction that occurs on the octahedral phase. Furthermore, NH_3 can be adsorbed on the hydroxyls (oxygen excess) of the tetrahedral phase as ammonium ions, these being the active SCR species on the tetrahedral phase.

At 125 °C the SCR reaction takes place via an ER mechanism, in which NO_2 (or the less reactive NO) reacts from the gas phase with the surface active NH_3 species. Two different SCR mechanisms are operative depending on the NH_3 species involved:

5.1. SCR by aminooxy groups

This is a steady-state mechanism. At 125 °C it comprises the following stages: (i) ammonia adsorption on oxygen atoms, (ii) the formation of aminooxy groups, (iii) SCR reaction between the aminooxy groups and the gas-phase NO (in the absence of oxygen) or NO_2 ($\sim$ three times faster than with NO) formed via nitrosyl oxidation with gas-phase oxygen, (iv) dehydroxylation of the octahedral phase, and (v) surface oxidation of the oxygen vacancies (nitrosyl reduction to N_2). The overall SCR process is $6NO + 4NH_3 \rightarrow 5N_2 + 6H_2O$.

5.2. SCR by ammonium ions

At 125 °C this is a pseudo-steady-state mechanism which initially accounts for $\sim$ 60% of the total NO reduction but it is gradually deactivated by the nitrates formed on the same hydroxyl groups that are available for ammonium formation. It comprises the following stages: (i) ammonium formation on the hydroxyl groups (oxygen excess) of the tetrahedral phase and (ii) SCR reaction between the ammonium ions and the gas-phase NO_2 formed as a result of nitrosyl oxidation with gas-phase oxygen. The overall SCR process is $4NO + 4NH_3 + O_2 \rightarrow 4N_2 + 6H_2O$.

At higher temperatures the mechanism evolves toward a limiting mechanism in which NO replaces NO_2 as the main reagent in the SCR reaction; reoxidation of the active phase is performed by gas-phase oxygen instead of NO/O_2, whereas nitrate formation does not take place at all since NO_2 is no longer available.

Acknowledgments

The authors gratefully acknowledge financial support from FEDER (1FD97-1636) and Hidroeléctrica del Cantábrico S.A; T. Valdés-Solís thanks the Government of the Principado de Asturias for the award of a predoctoral grant with funds from the Plan de Investigación, Desarrollo Tecnológico e Innovación de Asturias 2001–2004.

References

[1] M. Baldi, E. Finocchio, Ch. Pistarino, G. Busca, Appl. Catal. A 173 (1998) 61.
[2] A.M. Maltha, T.L.H. Favrem, H.F. Kist, A.P. Zuur, V. Ponec, J. Catal. 149 (1994) 364.
[3] S. Cimino, S. Colonna, S. De Rossi, M. Faticanti, L. Lisi, I. Pettiti, P. Porta, J. Catal. 205 (2002) 309.
[4] T. Valdés-Solís, G. Marbán, A.B. Fuertes, Catal. Today 69 (2001) 259.
[5] F. Kapteijn, L. Singoredjo, M. van Driel, A. Andreïni, J.A. Moulijn, G. Ramis, G. Busca, J. Catal. 150 (1994) 105.
[6] G. Marbán, A.B. Fuertes, Appl. Catal. B 34 (1) (2001) 43.
[7] G. Marbán, A.B. Fuertes, Appl. Catal. B 34 (1) (2001) 55.
[8] T. Valdés-Solís, G. Marbán, A.B. Fuertes, Appl. Catal. B 46 (2003) 261.
[9] W.S. Kijlstra, D.S. Brands, E.K. Poels, A. Bliek, J. Catal. 171 (1997) 208.
[10] W.S. Kijlstra, D.S. Brands, H.I. Smit, E.K. Poels, A. Bliek, J. Catal. 171 (1997) 219.
[11] G. Marbán, T. Valdés-Solís, A.B. Fuertes, Phys. Chem. Chem. Phys. 6 (2) (2004) 453.
[12] G. Marbán, A. Cuesta, Energy Fuels 15 (2001) 764.
[13] J. Muñiz, G. Marbán, A.B. Fuertes, Appl. Catal. B 23 (1999) 25.
[14] W.H. Lee, P.J. Reucroft, Carbon 37 (1) (1999) 21.
[15] F. Xie, J. Phillips, I.F. Silva, M.C. Palma, J.A. Menéndez, Carbon 38 (2000) 691.
[16] G.S. Szymański, Z. Karpiński, S. Biniak, A. Świątkowski, Carbon 40 (2000) 2627.
[17] A.R. Chughtai, M.M.O. Atteya, J. Kim, B.K. Konowalchuk, D.M. Smith, Carbon 36 (11) (1998) 1573.
[18] U.S. Ozkan, Y. Cai, M.W. Kumthekar, J. Catal. 149 (1994) 390.
[19] G.M. Robb, W. Zhang, P.G. Smirniotis, Micropor. Mesopor. Mater. 20 (1998) 307.
[20] S. Mrowec, in: C. Laird (Ed.), Materials Science Monographs, vol. 5, Elsevier, Amsterdam, 1980, p. 75.
[21] M. Inomata, A. Miyamoto, Y. Murakami, J. Catal. 62 (1980) 140.
[22] F. Janssen, F. van den Kerkhof, H. Bosch, J.J. Ross, Phys. Chem. 91 (1987) 5931.
[23] F. Janssen, F. van den Kerkhof, H. Bosch, J.J. Ross, Phys. Chem. 91 (1987) 6633.
[24] J. Marangozis, Ind. Eng. Chem. Res. 31 (1992) 987.
[25] M. Anstrom, N.-Y. Topsøe, J.A. Dumesic, J. Catal. 213 (2003) 115.
[26] D.F. Shiver, P.W. Atkins, Inorganic Chemistry 3.0, http://www.chem.ox.ac.uk/InorganicChemistry3/Mn/molecules/mn3o41.mol.
[27] G. Busca, L. Lietti, G. Ramis, F. Berti, Appl. Catal. B 18 (1998) 1.
[28] G. Marbán, R. Antuña, A.B. Fuertes, Appl. Catal. B 41 (2003) 323.
[29] G. Marbán, A.B. Fuertes, Catal. Lett. 84 (1) (2002) 13.
[30] U.S. Ozkan, Y. Cai, M.W. Kumthekar, J. Catal. 149 (1994) 375.
[31] A.M. Efstathiou, X.E. Verykios, Appl. Catal. A 151 (1997) 109.
[32] M.A. Larrubia, G. Ramis, G. Busca, Appl. Catal. B 30 (2001) 101.
[33] E.W.L. Chan, D.-Ch. Lee, M.-K. Ng, G. Wu, K.Y.C. Lee, L. Yu, J. Am. Chem. Soc. 124 (41) (2002) 12238.
[34] E.W.L. Chan, L. Yu, Langmuir 18 (2002) 311.
[35] S. Liu, A. Obuchi, J. Uchisawa, T. Nanba, S. Kushiyama, Appl. Catal. B 37 (2002) 309.
[36] G. Ramis, G. Busca, F. Bregani, F. Forzatti, Appl. Catal. 64 (1990) 259.
[37] R.Q. Long, R.T. Yang, J. Catal. 207 (2002) 274.
[38] R.Q. Long, R.T. Yang, J. Catal. 194 (2000) 80.
[39] R.Q. Long, R.T. Yang, J. Catal. 207 (2002) 224.